Chemical Geology 396 (2015) 164–181

Contents lists available at ScienceDirect

Chemical Geology

journal homepage: www.elsevier.com/locate/chemgeo

The origin of solutes within the groundwaters of a high Andean aquifer

Clinton Rissmann [a], Matthew Leybourne [b,*], Chris Benn [c], Bruce Christenson [d]

[a] Environment Southland, Invercargill, New Zealand
[b] Department of Earth Sciences and Mineral Exploration Research Centre, Laurentian University, 935 Ramsey Lake Rd, Sudbury, Ontario P3E 2C6, Canada
[c] Gold Fields Exploration, Vancouver, BC, Canada
[d] GNS Science, Lower Hutt, New Zealand

ARTICLE INFO

Article history:
Received 17 September 2013
Received in revised form 12 November 2014
Accepted 15 November 2014
Available online 8 January 2015

Editor: Michael E. Böttcher

Keywords:
Atacama Desert
Hyperarid
Groundwater geochemistry
Stable isotopes
Hydrothermal
Brines

ABSTRACT

This paper investigates the origin of solutes within the groundwaters of the Monturaqui–Negrillar–Tilopozo (MNT) aquifer system within the high Andes of the Atacama Desert that discharges into the Salar de Atacama. Key questions include the relative significance of volcanic hydrothermal processes and evaporitic brine recycling over solute supply as well as the pathways of solute ingress to the MNT aquifer system. Groundwaters were analysed for elemental (major, minor and trace) and isotopic ($\delta^{18}O/\delta^{2}H$; $\delta^{13}C$–DIC; $\delta^{34}S$–SO_4; $^{87}Sr/^{86}Sr$) constituents to which various hydrochemical and multivariate statistical methods have been applied. Groundwaters are all classified as thermal and show increasing temperatures (27–35 °C) and concentrations of HCO_3 (4.4–10.4 mmol L^{-1} dissolved inorganic carbon [DIC]) with increasing proximity to Volcano Socompa resulting from an increasing mass flux of steam and magmatic CO_2 (pCO_2 = 0.016 to 0.10 atm; $\delta^{13}C$–CO_2 = −9.3 to −3.6‰ (V-PDB)) boiled off a deep hydrothermal reservoir. Superimposed upon this gradational and relatively smooth spatial increase in heat and mass flow is a sharp, structurally controlled, increase in TDS (826–3632 mg l^{-1}) and a concomitant change in $\delta^{34}S$–SO_4 (+0.79 to 4.9‰ (V-CDT)) and $^{87}Sr/^{86}Sr$ values (0.707375–0.706859) associated with the inflow of evaporitic solutes. Evaporitic inputs are chemically and isotopically distinct from localised secondary hydrothermally derived solutes with major, minor and trace element data suggesting an origin within a highly oxidising, alkaline, evaporitic lake receiving dilute inflows enriched in volcanic/fumarolic sulfur mineralisation probably from volcanoes Socompa, Salín or Pular that delimit the eastern topographic extent of the aquifer system. The conceptual model presented in this paper proposes that basal leakage of evaporitic brines from active salar(s), within the high altiplano/volcanic arc, are actively entrained by sub-regional groundwater flow and conveyed to the MNT aquifer system where they mix with solutes derived from localised secondary hydrothermal gas–water–rock interaction. This work provides detail on the origin and processes controlling the solute composition of groundwater inflows to the Salar de Atacama within the volcanically active and hyperarid Atacama Desert and may be of significance to conceptual models of evaporitic brine evolution, recycling of evaporitic brines and hydrothermalism in arid regions.

1. Introduction

Historically, deciphering the origin and processes controlling the supply of solutes to the meteoric and volcanic-hydrothermal waters of the hyperarid Atacama Desert has been problematic. The main difficultly arises from the ubiquity of highly soluble evaporitic salts associated with active salt lakes (Risacher et al., 2003; Boschetti et al., 2007; Risacher and Fritz, 2008; Risacher et al., 2011) and massive volumes (~10,000 km^3) of anhydrite buried beneath the current day volcanic arc (Pueyo et al., 2001) both of which may be recycled through the hydrological cycle (Risacher et al., 2003; Banks et al., 2004) or via active volcanism either at the high temperatures of magma emplacement or during convective dissolution or entrainment by primary hydrothermal fluids (Youngman, 1984; Risacher and Alonso, 2001; Tassi et al., 2010). Further ambiguity arises through having to account for solutes derived from low temperature meteoric gas–water–rock processes including leaching of massive sulfide emplacements or volcanic/fumarolic sulfur mineralisation, and mixing with basinal brines or metamorphic fluids (Alpers and Whittemore, 1990; Banks et al., 2004; Cameron and Leybourne, 2005; Leybourne and Cameron, 2006). However, Risacher et al. (2003), Risacher and Fritz (2008) and Risacher et al. (2011) have demonstrated that 75–90% of the dissolved solute load within inflow waters, including thermal springs, supplying evaporitic lakes originate from the recycling of evaporitic brines.

This study seeks to decipher the origin and processes governing the solute composition of groundwaters within a high Andean aquifer that ultimately discharges to the Salar de Atacama. Given the potential for

* Corresponding author. Tel.: +1 705 675 1151x2263.
E-mail address: mleybourne@laurentian.ca (M. Leybourne).

http://dx.doi.org/10.1016/j.chemgeo.2014.11.029
0009-2541/

multiple solute sources, we have used a multi-element, multi-isotope and multivariate statistical approach to assess and constrain the source of solutes within the groundwaters of the MNT aquifer system.

2. Geology and hydrogeology

2.1. Climate

The Atacama Desert is considered the driest place on earth and has been arid to hyperarid since the early Oligocene (~45 Ma; e.g., Alpers and Brimhall, 1988; Arancibia et al., 2006; Clarke, 2006), although the timing of the onset of hyperaridity is debated (Hartley and Chong, 2002; Dunai et al., 2005; Hartley and Rice, 2005; Rech et al., 2006; Reich et al., 2009). Mean annual precipitation (MAP) ranges from <1 mm yr^{-1} within the central desert (Pampa del Tamarugal) to ~150–200 mm yr^{-1} along the volcanic front (>4500 m a.s.l. [above sea level]) (Magaritz et al., 1989, 1990; Drees et al., 2006). In all regions, potential evaporation rates greatly exceed MAP, varying from >1500 mm yr^{-1} in the central desert to 600–1200 mm yr^{-1} along the volcanic front (Risacher et al., 2003).

For the Monturaqui–Negrillar–Tilopozo area, MAP ranges from ~40 mm yr^{-1} at 3100 m a.s.l. to ~100 mm yr^{-1} at 4000 m a.s.l (Quade et al., 2007). Therefore, precipitation events of sufficient magnitude to overcome evaporative thresholds and result in recharge are typically restricted to the current day volcanic arc and eastern altiplano. The majority of this precipitation is derived from intense (≥100 mm), long return storm events (~5 year cyclicity; Drees et al., 2006) associated with the South American Summer Monsoon (SASM) that traverse the South Central Andes and bring precipitation to the western altiplano and volcanic arc (Miller, 1976; Aravena et al., 1999). Impounded behind the volcanic arc ephemeral streams recharged during SASM storm events flow into endorheic basins where a number of variably sized (~20 km^2 to 1600 km^2) saline lakes occur.

2.2. Geology

2.2.1. Evolution of MNT trough and aquifer system

The Monturaqui–Negrillar–Tilopozo (MNT) trough is a 60 km long N–S oriented depression that formed contemporaneously with the Miocene–Holocene eruption of the present magmatic arc (or Western Cordillera) (Fig. 1; Bock et al., 2000). The stratigraphy and hydrostratigraphy of the MNT aquifer system is summarised in Table 1. The eastern extent of the MNT trough is defined by young (Pleistocene) Andean type stratovolcanoes of the current day volcanic arc whereas the western extent is controlled by the N–S trending Late Proterozoic Arequipa–Anotofalla basement anticlines of the Sierra Almeida, Sierra Agua Colorada and the Cordon de Lila ranges. The trough is divided into the southern Monturaqui Basin, the central Negrillar and the northern most Tilopozo zones (Wadge et al., 1995; van Wyk de Vries et al., 2001), where the Domeyko Range becomes the western most margin of the Preandean depression.

Emplacement of the current volcanic arc was followed by an ignimbrite flare-up in the Late Miocene–Pliocene, during which the MNT trough was filled with 200–300 m of volcanic ash and ignimbrite, forming the Salín Formation, the principal aquifer of the structural trough. The Salín Formation extends eastward behind the modern day volcanic arc where it outcrops at higher elevations across the altiplano, forming an extensive permeable ignimbrite sheet (Wadge et al., 1995; van Wyk de Vries et al., 2001; Anderson et al., 2002).

2.2.2. Salín Formation

The Salín Formation aquifer is characterised by a poorly consolidated mix of volcaniclastic sediments that are predominantly of dacitic composition, ranging from fine to medium grained sands, significant ash deposits, local discontinuous gravel horizons, ignimbrite sequences, and conglomerates (van Wyk de Vries et al., 2001; Anderson et al., 2002). Gravels and conglomerates are supported within a matrix of volcanic

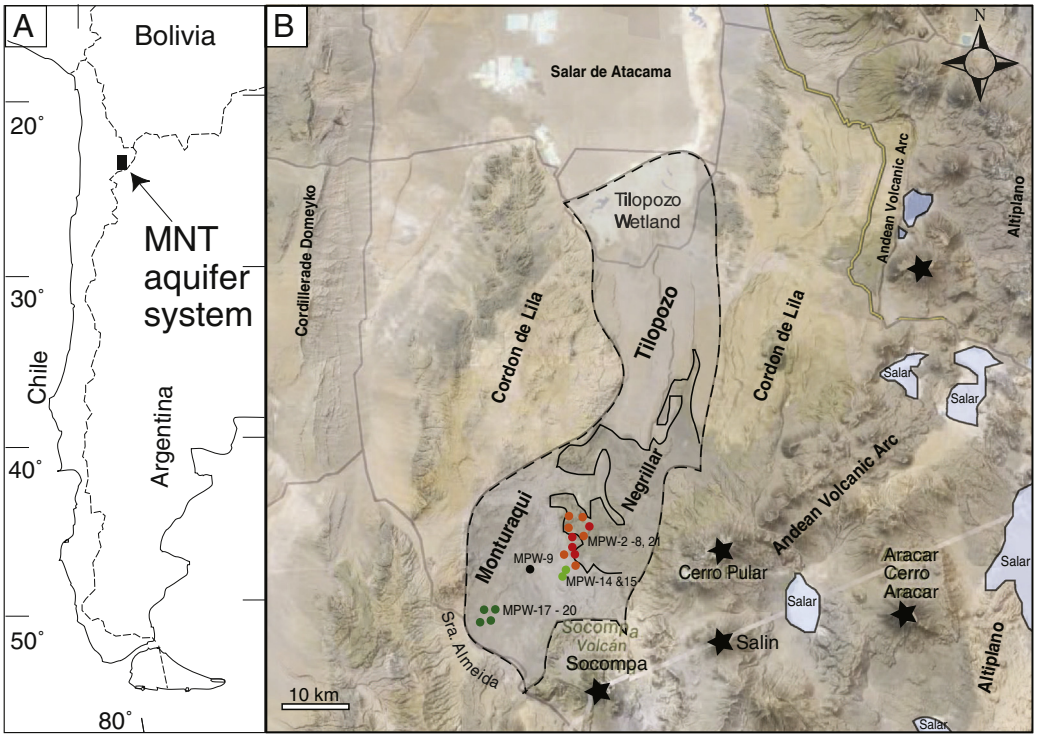

Fig. 1. Location of Socompa. (a) Location of MNT aquifer system in South America; (b) hydrogeological setting of MNT aquifer system. The extent of the MNT aquifer system is depicted by the dotted line and includes the Monturaqui Valley, the Negrillar Volcanics, and the Tilopozo sections of the aquifer system. The Tilopozo Wetland constitutes the discharge point for groundwater from the MNT aquifer into the Salar de Atacama. Stars identify volcanoes Socompa (6051 m), Salín, Pular and Aracar within the current volcanic arc. Salars are impounded behind and within the volcanic arc and altiplano — small salars not shown. Production wells are shown as coloured circles, with colours denoting water type as per the classification of Section 4.3. (For interpretation of the references to colour in this figure legend, the reader is referred to the web version of this article.)

Table 1
Stratigraphy and hydrostratigraphy of the Monturaqui–Tilopozo–Negrillar aquifer system (Anderson et al., 2002).

Unit (age)	Thickness (m)	Stratigraphy	Hydrostratigraphy
Alluvium, volcanic ash and debris (Recent)	0–50	Reworked sediments from other formations. Rhyolitic tuff and lava blocks from eruption of Volcano Socompa	Unsaturated, except near Tilopozo wetland
El Negrillar Volcanics	0–100	Lava flows overlying significant areas of the Salín, particularly on the basin margins and forming the topographic between the Monturaqui and Negrillar areas	Low Permeability vents and dykes
Tucucaro ignimbrite (Pliocene)	0–50	Strongly welded white-grey ignimbrite forming part of a suite of undifferentiated volcanic rocks. Overlies the Slain Forma on in the northern part of the basin	Possible confining layer in the northern part of the aquifer where it is not fractured
Estratos de Quebrada Salín (Salín) (Miocene to Pleistocene)	100–200	Poorly consolidated clastic sediments, ignimbrite and ash deposits which unconformably overlie the Purilactus Formation and crop out where not covered by more recent volcanics. In the Monturaqui area, the Salín sediments generally consist of fine to medium grained sands with significant ash contents and local discontinuous gravel horizons. In the Negrillar area a higher fraction of coarse material and stratification is evident.	Primary aquifer with large thickness of medium to high permeability material. Upper and lower zones are recognised in Monturaqui.
Purilactus Forma on (late Cretaceous/early Tertiary)	100–300	Comprises continental sediments unconformably overlying the Palaeozoic basement, consisting predominantly of silt with as and only occasional thin sand layers. Crops out in a limited area to the west of the Monturaqui Basement.	Low permeability
Palaeozoic rocks	Basement	Metamorphosed marine sediments, volcanics and intrusives subject to all four structural phases. Host to the MNT basin.	Extremely low permeability

ash, large pumice clasts (up to 10 cm) are common, and sand-rich layers of up to 10 m in thickness and hundreds of metres long are extensive throughout the Basin (van Wyk de Vries et al., 2001; Anderson et al., 2002). In the Negrillar area a higher fraction of coarse materials is evident.

The upper units of the Salín Formation (ignimbrites and volcaniclastics) are chemically similar to Socompa lavas suggesting these units were derived from the volcano (Déruelle, 1978a,b; van Wyk de Vries et al., 2001). A similar magma source for ignimbrites and lavas is a common feature of the south central Andes (Déruelle and Moorbath, 1993).

2.2.3. Volcano Socompa & El Negrillar Volcanics

Numerous volcanic complexes, including Volcano Socompa (6051 m) and the low altitude (~3200 m) El Negrillar volcanics, active during the late Pliocene and Pleistocene, intruded into and flowed over the Salín Formation (van Wyk de Vries et al., 2001; Anderson et al., 2002). The Pleistocene El Negrillar Volcanics overlie large areas of the Salín Formation, forming a prominent topographic boundary between the Monturaqui and Negrillar portions of the MNT trough (Fig. 1). The geochemistry of the Negrillar lavas, andesite and basaltic-andesite, differs markedly from the dacitic composition of the much more voluminous Salín Formation and are notable for elevated Cr, Rb, Sr, Ba, Ni, Ta, Th and U contents (Déruelle, 1978a,b; Déruelle et al., 1996).

Volcano Socompa is situated at the head of the MNT aquifer system (Fig. 1) and is the youngest and westernmost member of a NE–SW trending chain of large (~6000 m a.s.l) Andean type stratovolcanoes (Wadge et al., 1995; van Wyk de Vries et al., 2001). Eruptive activity has typically been of stubby dacitic and andesitic lava flows from the central cone, with lesser ignimbrites, plinian pumice deposits and dacite domes (Wadge et al., 1995; van Wyk de Vries et al., 2001). Lavas from Socompa built up on top of the Salín Formation during the Pleistocene and blocked what was once a broad valley descending from the east (Fig. 1) (van Wyk de Vries et al., 2001). The growing volcanic edifice resulted in extrusion and thinning of the saturated, poorly to unconsolidated Salín Formation sediments from beneath Socompa, causing sagging, faulting of the volcanic edifice and eventual collapse ~7200 years B.P. (Francis et al., 1985; Wadge et al., 1995; van Wyk de Vries et al., 2001).

Although unlisted among active south-central Andean volcanoes (de Silva and Francis, 1991), Socompa exhibits little evidence of glaciation, with fresh volcanic features and little erosion (van Wyk de Vries et al., 2001). The last known eruptive activity, the formation of dome complexes within the collapse scar, is dated at ~5250 yr B.P. (Siebert and Simkin, 2002). Recent work by Costello et al. (2009) identified minor areas of anomalous CO_2 and CH_4 soil gas anomalies about the summit of Socompa. Anomalous soil temperatures and steam vents were also detected, although the concentration of gas measured and the reported heat flow anomalies were minor compared to active volcanoes or volcanic-hydrothermal fields globally (Rissmann et al., 2012 and references therein). Costello et al. (2009) also reported the odour of H_2S about the areas of diffuse degassing. Socompa therefore shows some evidence of geologically recent activity and current anomalous gas and heat flow signatures consistent with a deep-seated heat source in some state of repose.

2.2.4. Salars

The eastern flanks of the volcanoes Socompa, Salín, Pajonales and Pular form the eastern boundary of the MNT structural trough behind which a number of large evaporitic salars are impounded (Fig. 1). Here within the high Altiplano/arc (>4000 m a.s.l.), evaporitic brines within the nucleus of the larger salars extend to depths of up to 400 m or more within the permeable layers of the Salín Formation, well beneath the water table (e.g., Kesler et al., 2012).

2.3. Geohydrology

2.3.1. MNT aquifer system

Investigations into the hydrogeology of the MNT aquifer system are provided by Karim (1998) and Anderson et al. (2002) and the hydrostratigraphy of the aquifer is summarised in Table 1. The Salín Formation varies in thickness from ~200 m within the MNT aquifer system, to ~150 m below Volcano Socompa and greater than 300 m at higher elevations to the east of the volcanic arc. Saturated thickness ranges from ca. 150 m in Monturaqui to 450 m in Negrillar. The aquifer system is at its widest within the Monturaqui section (ca. 12 km), narrowing to just 3 km north of Negrillar and widening again to 8 km in the Tilopozo area (Fig. 1). The MNT aquifer system hosts an estimated 10^{10} m^3 of water (Anderson et al., 2002).

Groundwater flow is from south to north, with hydraulic gradients ranging from 0.005 in Monturaqui to 0.05 north of Negrillar, due to the constriction in the aquifer north of Negrillar. Aquifer through flow is estimated at approximately 400 l s^{-1} in the Monturaqui area, increasing to approximately 900 l s^{-1} in the Negrillar and Tilopozo areas. Transmissivity values range between 500 and 2500 m^2 d^{-1} within the Monturaqui–Negrillar section of the MNT aquifer and increase to 3000–4500 m^2 d^{-1} down gradient

of Negrillar. Hydraulic conductivity ranges between 1.6 and 10 m d^{-1} throughout the length of the basin (Anderson et al., 2002).

Pump tests indicate medium to high permeability and response characteristic of a semi-confined (leaky) aquifer (Karim, 1998). Around Negrillar the intrusion of low permeability vents and dykes through the Salín Formation produces localised barriers to groundwater flow, which partially but not wholly, disrupts the continuity of the Salín Formation aquifer (Anderson et al., 2002). The aquifer gradually wedges out towards the Tilopozo discharge area, as it flows over the denser brines of the Salar de Atacama (Fig. 1). The Tilopozo wetland is the sole natural discharge zone of the MNT aquifer system with discharge estimates of between 400 and 900 l s^{-1} (Anderson et al., 2002). Discharge is affected by evapotranspiration from vegetation, springs, saline lagoons and bare ground that cover an area of approximately 38 km^2.

The groundwater table varies from −124.7 to −67.9 m below ground level (b.g.l.) whereas the screened interval for all wells varies between −136.0 and −208.0 m b.g.l (Anderson et al., 2002; BHP-Billiton unpublished data on the MNT well field). Water table depth increases towards Volcano Socompa whereas screened intervals are deepest immediately south of the Negrillar Volcanics. Mean and median groundwater level are −103.8 and −105.3 m b.g.l., respectively. Mean and median screen interval depth is −177.4 and 177.0 m b.g.l., respectively.

2.3.2. Recharge

The two principal sources of recharge to the MNT aquifer system include: (i) shallow groundwater inputs via sediment-filled high altitude valleys associated with the large stratovolcanoes that form the eastern margin of the MNT, and (ii) subregional groundwater inflow via the highly permeable Salín Formation that outcrops at high (>4000 m) elevations (altiplano) to the east of the volcanic front (Fig. 1; Karim, 1998; van Wyk de Vries et al., 2001; Anderson et al., 2002). Groundwater recharge from the western ranges of the Sierra Almedia and Sierra Agua Colorada is considered negligible (Anderson et al., 2002).

A significant component of recharge originates beyond the topographic extent of the MNT aquifer system with Anderson et al. (2002) using the recharge component originating in the high Altiplano via the Salín Formation to explain the discrepancy between recharge estimates (ca. 250 l s^{-1}), calculated on the basis of the topographic extent of the MNT aquifer system, and discharge at the Tilopozo wetland (ca. 400–900 l s^{-1}). The extension of recharge zones beyond the topographic boundary of a catchment, and sub-regional to regional groundwater flow paths, is a common phenomenon of the central Andes, where older aquifers are intruded by later sequences of igneous rocks (Magaritz et al., 1990; Anderson et al., 2002).

3. Methods

3.1. Field sampling

In order to characterise the geochemistry of Monturaqui groundwaters, field measurements and water samples were collected for laboratory analyses from 17 large volume (>100 l s^{-1}) production wells within the Monturaqui–Negrillar areas of the MNT aquifer system (Fig. 1; Tables 2–4). Samples were taken at each pump site through bleeder valves. Duplicate samples and field blanks were also included during sampling. Typically, pumps were run for at least 5 h before sampling. Temperature (°C), pH, Eh, dissolved oxygen (D.O.), and SpC (specific conductivity) were measured at each well using two meter-and-electrode combinations to reduce the chance of error during sampling. Note that the turbulent flow induced by bleed valves compromises the value of D.O. for assessing groundwater redox state. Filtered cation (FC) and filtered anion (FA) splits were taken using 0.45 μm Millipore MF filters. Specific sampling for analysis of stable isotopes of carbon, oxygen, hydrogen and the $^{87}Sr/^{86}Sr$ isotopes was also undertaken. Aqueous sulfate was precipitated as $BaSO_4$ and separated onto non-reactive filters for sulfur isotope analysis. Cation samples were acidified to 1% by volume with ultra-pure HNO_3. An unfiltered, unacidified split was taken for additional anion and alkalinity determinations.

3.2. Laboratory analysis

Major and minor cations (S, Si, Fe, Mg, Ca, Na, K, B, Mn, Sr, and Cu) were analysed by inductively coupled plasma optical emission spectrometry (ICP-OES; Perkin Elmer Optima 3300 DV), trace elements (Li, Co, Cr, Cs, Fe, Mn, Pb, Rb, Sb, U, V, Al, Ba, Cd, Cu, Mo, As, Ni, Se, Zn, Sr, Re, and Th) by mass spectrometry (ICP-MS; Perkin Elmer-Sciex Elan 6100 DRC), anions (SO_4, NO_3, Cl, Br, and F) by ion chromatography (IC; Dionex DX600), and alkalinity by end-point titration with H_2SO_4 (Orion 950 titrator) at the Geosciences Department, University of Texas at Dallas. Alkalinity was not measured in the field, but was determined as soon as the samples were returned to the US. Total alkalinity is conservative, so that loss of CO_2 from the sample bottles will not affect total alkalinity. Most samples had low Fe contents (<1 mg/l) so that precipitation of $Fe(OH)_{3(s)}$ likely had little impact on total alkalinity. Accuracy and precision were determined by running certified standard reference materials (NIST 1640 or NIST 1643). Analyses were quantified using external calibration (SCP Science certified standards) and ICP-MS analyses were drift-corrected by running a systematic drift standard after each five unknowns and adjusted using a modified method of Cheatham et al. (1993). Precision was assessed by repeated analysis of NIST 1640/1643 and was generally better than 2% for ICP-ES and MS analyses. Bromine and I were also measured by ICP-MS. Electrical balances are excellent with all waters showing less than 5% difference between cations and anions.

Stable isotopes were measured at the G.G. Hach Stable Isotope Laboratory in the Department of Earth Sciences, University of Ottawa (oxygen, hydrogen, carbon, and sulfur) with additional sulfur isotopes measured at the Department of Physics and Astronomy at the University of Calgary. For deuterium analyses, 3 μl of sample was trapped by liquid nitrogen under vacuum (<10 mT) in Pyrex breakseals with 100 mg of zinc. Samples were baked at 500 °C for 30 min before analysis on a Micromass 602E mass spectrometer. Two standards were run for every eight unknowns and the data reduced by linear regression to account for variations in oxidation of zinc and changes in the reference gas. Oxygen isotopes were analysed on a VG Isogas Sira 12 mass spectrometer, using 1 ml sample aliquots. Samples were equilibrated with CO_2 gas for 6 h prior to analysis. However, for samples with salinities >10% TDS (total dissolved solids) equilibration times were increased to 36–48 h to allow for the greater hydration sheath of ions in high salinity solutions. During a typical analytical run, 16–17 samples were run with three or four standards and the data corrected by linear regression on the standards. Carbon isotopes were analysed on the total dissolved inorganic carbon (DIC) component. Stable carbon isotopes were measured by converting the DIC to CO_2 with 100% phosphoric acid (H_3PO_4) followed by cryogenic separation and analysis by mass spectrometry on a VG Isogas Sira 12 mass spectrometer. Sulfur isotopes were measured by mass spectrometry following precipitation of sulfate as $BaSO_4$. For hydrogen analyses, reproducibility is typically better than ±2‰, for oxygen, better than ±0.1‰, for carbon, ±0.2‰ and for sulfur, ±0.7‰. For S isotopes at the University of Calgary, reproducibility is typically better than ±0.5%, on the basis of replicate analyses of CRMs NBS 127, IAEA S-1, and IAEA S-2. The $\delta^{18}O$ and $\delta^{2}H$, $\delta^{13}C$, and $\delta^{34}S$ values are expressed in ‰, relative to V-SMOW, V-PDB and V-CDT reference standards, respectively.

Strontium isotopes were determined at UTD. Sr was precipitated as $SrCO_3$ by adding a 1 M $NaCO_3$ solution to sample aliquots. The precipitate was dissolved in 1 N HNO_3 and the strontium separated using a strontium specific ion exchange resin. The isotope ratios were measured on a second order, double focusing mass spectrometer with a 60°, 33.0 cm radius of curvature magnetic sector and a 91°, 40.1 cm radius of curvature electric sector. Masses 85, 86, 87, and 88 were measured

Table 2
Field, isotopic and modelled parameters for MNT aquifer system.

Sample ID	Lat	Long	Cluster	Distance Socompa	T	pH	Eh	SpC	TDS	Steam	CO_2 (g)	pCO_2	$\delta^{13}C$–DIC	$\delta^{13}C$–CO_2	^{34}S–SO_4	D–H_2O	^{18}O–H_2O	$^{87}Sr/^{86}Sr$
				km	°C		mV	μS/cm	mg/kg	Fugacity	Fugacity	(fugacity)	‰ (VPDB)	‰ (VPDB)	‰ (VCDT)	‰ (VSMOW)	‰ (VSMOW)	
MPW-11	24°12′45.99″S	68°17′30.11″W	1A	20.3	26.8	7.4	−143	850	1215	0.035	0.010	0.016						
MPW-8	24°12′23.23″S	68°17′38.29″W	1A	21.0	28.5	7.7	−75	950	1071	0.038	0.006	0.023	−1.7	−8.7	0.8	−58.8	−7.4	0.707375
MPW-5	24°11′17.85″S	68°16′44.32″W	1A	22.8	30.7	7.9	−126	940	819	0.043	0.005	0.024	−2.3	−9.3		−63.9	−8.2	
MPW-21	24°11′51.40″S	68°17′38.29″W	1A	22.1	28.0	7.6	−74	950	1216	0.037	0.007	0.026						
Median				21.5	28.3	7.6	−101	945	1143	0.038	0.007	0.023	−2.0	−9.0	0.8	−61.3	−7.8	0.707375
Mean				21.6	28.5	7.6	−105	923	1080	0.038	0.007	0.022	−2.0	−9.0	0.8	−61.3	−7.8	0.707375
MPW-4	24°11′19.54″S	68°17′48.27″W	1B	22.9	27.8	7.8	−60	1150	954	0.037	0.006	0.027	−1.4	−8.5	1.8	−61.2	−7.5	
MPW-10	24°12′46.78″S	68°18′4.44″W	1B	20.8	29.8	7.6	−139	1810	1219	0.041	0.009	0.038	0.7	−6.0	2.3	−60.1	−7.6	
MPW-2	24°10′45.03″S	68°17′53.82″W	1B	24.1	26.5	7.6	−125	1590	1219	0.034	0.009	0.038	−0.7	−7.8	1.9	−59.8	−7.5	0.707337
MPW-3	24°10′45.19″S	68°17′3.08″W	1B	23.8	28.2	7.7	−60	1130	1486	0.037	0.008	0.046	−0.8	−7.5		−67.6	−8.3	
MPW-7	24°11′48.00″S	68°17′2.52″W	1B	21.9	31.9	7.5	−60	1730	1299	0.046	0.015	0.049	−1.0	−7.3		−62.4	−8.1	0.707348
MPW-13	24°13′21.50″S	68°17′28.00″W	1B	19.1	27.8	7.6	−72	1320	1097	0.037	0.012	0.058	−1.1	−7.9		−54.6	−7.7	
Median				22.4	28.0	7.6	−66	1455	1219	0.037	0.009	0.042	−0.9	−7.7	1.9	−60.7	−7.6	0.707343
Mean				22.1	28.7	7.6	−86	1455	1212	0.039	0.010	0.043	−0.7	−7.5	2.0	−61.0	−7.8	0.707343
MPW-14	24°13′34.93″S	68°17′58.54″W	2B-1	18.9	29.5	7.6	−156	1810	1434	0.040	0.013	0.081						0.707198
MPW-15	24°13′55.92″S	68°18′9.26″W	2B-1	18.2	31.6	7.3	−170	2150	1784	0.046	0.030	0.105	−0.7	−6.5		−62.0	−7.9	
Median				18.5	30.6	7.4	−163	1980	1609	0.043	0.021	0.093	−0.7	−6.5		−62.0	−7.9	0.707198
Mean				18.5	30.6	7.4	−163	1980	1609	0.043	0.021	0.093	−0.7	−6.5		−62.0	−7.9	0.707198
MPW-9	24°13′33.02″S	68°19′51.74″W	2A	20.3	30.1	7.5	150	6660	3593	0.042	0.012	0.060	−1.1	−7.3	4.3	−54.6	−7.7	0.706859
MPW-18	24°15′39.88″S	68°21′36.62″W	2B-2	18.6	34.6	7.4	−42	2500	1905	0.054	0.018	0.039			4.8			
MPW-17	24°15′40.94″S	68°22′17.03″W	2B-2	19.3	32.2	7.1	−65	1900	1609	0.047	0.024	0.047						
MPW-19	24°16′28.82″S	68°22′34.64″W	2B-2	18.8	33.8	6.8	−41	1880	1533	0.051	0.046	0.059	0.1	−3.6	4.2	−64.6	−8.1	0.706935
MPW-20	24°16′14.96″S	68°21′55.68″W	2B-2	18.1	33.0	7.4	−27	2430	1850	0.049	0.016	0.063	−0.4	−5.5	4.9	−60.2	−8.3	
Median				18.7	33.4	7.2	−42	2165	1730	0.050	0.021	0.053	−0.2	−4.5	4.8	−62.4	−8.2	0.706935
Mean				18.7	33.4	7.1	−44	2178	1724	0.050	0.026	0.052	−0.2	−4.5	4.6	−62.4	−8.2	0.706935

Table 3
Field parameters and major and minor species for MNT aquifer system.

Sample ID	Cluster	Distance Socompa	T	pH	Eh	SpC	TDS	Li	Na	K	Rb	Cs	Mg	Ca	Sr	Ba	F	Cl	SO_4	SiO_2 (aq)	Alk.
		km	°C		mV	µS/cm	mg/kg	µg/l	mg/l	mg/l	µg/l	µg/l	mg/l	mg/l	µg/l	µg/l	µg/l	mg/l	mg/l	mg/l	mg/l
MPW-11	1A	20.3	26.8	7.4	−143	850	1215	261	90	8.3			28	59	330	32	940	86	132	43	266
MPW-8	1A	21.0	28.5	7.7	−75	950	1071	283	97	9.1			28	76	354	65	850	91	128	43	325
MPW-5	1A	22.8	30.7	7.9	−126	940	819	230	83	6.6			33	85	581	45	441	76	98	43	388
MPW-21	1A	22.1	28.0	7.6	−74	950	1216	281	93	8.6	13.6	1.1	27	76	346	39	630	87	129	43	313
Median		21.5	28.3	7.6	−101	945.0	1143.0	271	91	8.4	13.6	1.1	28	76	350	42	740	87	129	43	319
Mean		21.6	28.5	7.6	−105	923	1080	264	91	8.1	13.6	1.1	29	74	403	45	715	85	122	43	323
MPW-4	1B	22.9	27.8	7.8	−60	1150	954	314	107	9.0	15.0	0.5	30	108	424	22	511	105	148	41	406
MPW-10	1B	20.8	29.8	7.6	−139	1810	1319	532	172	14.0	23.6	2.7	61	153	369	25	539	144	258	46	445
MPW-2	1B	24.1	26.5	7.6	−125	1590	1219	482	158	13.9	24.4	1.8	46	125	664	25	410	214	198	44	442
MPW-3	1B	23.8	28.2	7.7	−60	1130	1486	420	133	11.2	19.2	2.1	50	115	614	44	360	154	125	45	454
MPW-7	1B	21.9	31.9	7.5	−60	1730	1299	534	163	14.2	23.2	2.6	59	144	860	15	343	211	187	48	515
MPW-13	1B	19.1	27.8	7.6	−72	1320	1097	376	124	12.0	18.1	1.4	39	117	506	24	590	138	165	44	470
Median		22.4	28.0	7.6	−66	1455	1259	451	146	13.0	21.2	1.9	48	121	560	24	461	149	176	45	450
Mean		22.1	28.7	7.6	−86	1455	1229	443	143	12.4	20.6	1.9	48	127	573	26	459	161	180	45	455
MPW-14	2B-1	18.9	29.5	7.6	−156	1810	1434	211	183	16.7			56	118	636	63	900	220	299	41	534
MPW-15	2B-1	18.2	31.6	7.3	−170	2150	1784	710	217	19.7			89	161	1280	22	1050	305	306	48	637
Median		18.5	30.6	7.4	−163	1980	1609	461	200	18.2			72	139	958	43	975	263	302	44	586
Mean		18.5	30.6	7.4	−163	1980	1609	461	200	18.2			72	139	958	43	975	263	302	44	586
MPW-9	2A	20.3	30.1	7.5	150	6660	3593	2870	1040	78.3	46.2	31.7	143	291	3170	38	4320	1100	612	53	442
MPW-18	2B-2	18.6	34.6	7.4	−42	2500	1905	1065	365	24.7	50.2	7.9	60	120	725	78	1410	385	477	51	442
MPW-17	2B-2	19.3	32.2	7.1	−65	1900	1609	698	216	16.1	28.7	8.0	61	131	670	50	880	205	519	51	339
MPW-19	2B-2	18.8	33.8	6.8	−41	1880	1533	702	214	16.1	27.6	8.0	62	134	672	40	720	191	484	51	353
MPW-20	2B-2	18.1	33.0	7.4	−27	2430	1850	1050	337	25.1	51.2	7.4	63	123	710	25	1290	359	465	52	430
Median		18.7	33.4	7.2	−42	2165	1730	876	276	20.4	39.5	7.9	61	127	691	45	1085	282	481	51	392
Mean		18.7	33.4	7.1	−44	2178	1724	879	283	20.5	39.4	7.8	61	127	694	48	1075	285	486	51	391

simultaneously in four separate faraday cups. The $^{87}Sr/^{86}Sr$ values have been normalised to $^{86}Sr/^{88}Sr = 0.1194$. The isotope ratio of the unknown samples was measured by comparison to a standard (Burke and Hetherington, 1984). The standard used was NBS 987 for which a value of 0.710240 has been assumed. More than 100 measurements of modern seawater yield a weighted mean of 0.709173 ± 3. This difference and values of standards compares well with results from other workers (see summary of McArthur and Howarth, 2004). All published results have been normalised to these values.

3.3. Chemical, isotopic and statistical modelling

Modelling of mineral solubility under the physiochemical conditions of the groundwaters at each well was undertaken using the software package The Geochemist's Workbench® (GWB) (Bethke, 2008), release 9.0.8, using the thermodynamic database "thermo.dat" (Delany and Lundeen, 1989). The theoretical pCO_2 of MNT groundwaters was calculated manually using the activity of HCO_3^- (derived from titrated alkalinities and speciation modelling

Table 4
Field parameters and trace species for MNT aquifer system.

Sample ID	Cluster	Eh	SpC	TDS	V	Cr	Mn	Fe	Co	Ni	Cu	Zn	Mo	Re	Al	As	U	Se
		mV	µS/cm	mg/kg	µg/l	µg/l	µg/l	µg/l	µg/l	µg/l	µg/l	µg/l	µg/l	µg/l	µg/l	µg/l	µg/l	µg/l
MPW-11	1A	−143	850	848				16					7.9					
MPW-8	1A	−75	950	892				41					8.1					
MPW-5	1A	−126	940	906				5					7.0					
MPW-21	1A	−74	950	872	29	4.8	30.6	1230	0.5	45	4.0	0.9	8.8	0.01	1.1	62	0.3	1.3
Median		−101	945	882	29	4.8	30.6	28	0.5	45	4.0	0.9	8.0	0.01	1.1	62	0.3	1.3
Mean		−105	923	879	29	4.8	30.6	323	0.5	45	4.0	0.9	7.9	0.01	1.1	62	0.3	1.3
MPW-4	1B	−60	1150	1044	28	5.8	66.0	786	0.2	18	1.9	1.9	11.8	0.01	2.0	79	0.5	1.0
MPW-10	1B	−139	1810	1292	29	7.4	22.0	405	0.5	36	0.9	1.9	12.2	0.02	1.7	47	1.4	2.1
MPW-2	1B	−125	1590	1337	36	14.2	15.4	8	0.2	19	1.1	1.4	11.4	0.02	1.4	175	1.4	2.3
MPW-3	1B	−60	1130	1187	26	7.4	65.0	1574	0.2	16	0.7	1.2	11.3	0.01	1.4	68	1.1	1.6
MPW-7	1B	−60	1730	1451	28	8.4	20.8	6000	0.5	38	0.8	2.3	9.7	0.02	2.0	110	1.3	2.0
MPW-13	1B	−72	1320	1205	38	7.4	35.8	1422	0.6	41	1.1	1.9	10.7	0.01	2.5	101	0.7	1.8
Median		−66	1455	1248	28	7.4	28.9	1104	0.3	27	1.0	1.9	11.4	0.02	1.9	90	1.2	1.9
Mean		−86	1455	1253	31	8.4	37.5	1699	0.4	28	1.1	1.8	11.2	0.02	1.8	97	1.1	1.8
MPW-14	2B-1	−156	1810	2455				33					14.7					
MPW-15	2B-1	−170	2150	2036				56					15.1					
Median		−163	1980	2246				44					14.9					
Mean		−163	1980	2246				44					14.9					
MPW-9	2A	150.0	6660	4056	119	12.1	1.1	78	0.5	41	5.6	7.3	302.0	0.22	16.5	1075	1.9	7.1
MPW-18	2B-2	−42	2500	2036	62	7.9	0.6	21	0.2	25	2.4	2.9	51.0	0.02	2.8	424	1.8	2.9
MPW-17	2B-2	−65	1900	1648	40	5.5	1.5	35	0.2	18	2.0	7.7	19.3	0.02	4.2	260	0.9	2.0
MPW-19	2B-2	−41	1880	1620	41	5.9	0.5	18	0.2	19	1.8	3.4	19.4	0.02	1.8	252	1.0	1.7
MPW-20	2B-2	−27	2430	1975	66	8.7	1.3	36	0.2	23	1.9	3.6	51.0	0.03	4.0	407	1.7	3.1
Median		−42	2165	1812	52	6.9	1.0	28	0.2	21	1.9	3.5	35.2	0.02	3.4	334	1.4	2.5
Mean		−44	2178	1820	52	7.0	1.0	28	0.2	21	2.0	4.4	35.2	0.02	3.2	336	1.4	2.4

within GWB), pH and temperature (°C) following the method of Macpherson, (2009):

$$\log_{10}(pCO_2) = \log_{10}(HCO_3^-) - pH + C_t \quad (1)$$

where $C_t = \log_{10}(K_{1,T}) - \log_{10}(K_{h,T})$, pH is in standard pH units ($-\log_{10}$ of the activity of H^+), HCO_3^- has units of chemical activity, $K_{1,T}$ is the temperature-dependent first association constant of $H_2CO_3^{0,*}$ (the sum of $H_2CO_3^0$ and CO_2^0) and $K_{h,T}$ is the temperature dependent Henry's Law constant expressing the relation between $H_2CO_3^{0,*}$ and pCO_2. The theoretical equilibrium $\delta^{13}C$–CO_2 signature of the original CO_2 source dissolved in the shallow meteoric aquifer was determined using the methodology of Federico et al. (2002) and the CO_2–DIC isotopic equilibrium equation of Zhang et al. (1995):

$$\delta^{13}C_{(CO_2)g} = \delta^{13}C_{(TDC)} - \frac{H_2CO_3}{TDC}\varepsilon(H_2CO_3 - CO_2) - \frac{HCO_3^-}{TDC}\varepsilon(HCO_3^- - CO_2) - \frac{CO_3^{2-}}{TDC}\varepsilon\left(CO_3^{2-} - CO_2\right). \quad (2)$$

Eq. (1) uses the measured isotopic signatures of $\delta^{13}C_{DIC}$ for the MNT aquifer system to determine the theoretical equilibrium $\delta^{13}C$–CO_2 signature of the original CO_2 source dissolving within the groundwaters and corrects for any possible temperature and/or pH-dependant isotopic fractionation effect during water–gas interaction (Federico et al., 2002). $\delta^{13}C_{DIC}$ values for MNT aquifer groundwaters were combined with the equilibrium molar ratios of aqueous carbon species and the isotope enrichment factors (ε) for dissolved carbon species and gaseous CO_2 at the sampling pH and temperature.

A two component mixing equation (Katz et al., 1998) was used to estimate the relative amount of influent saline groundwater in well field samples. For a two-component mixture, the fraction of saline inflow is defined as:

$$F_{saline} = (C_{MPWx} - C_{met})/(C_{saline} - C_{MPWx}) \quad (3)$$

where: C_{MPWx} = the concentration of the solute of interest in the groundwater sample (mixed); C_{met} = the concentration of the solute of interest in the meteoric end member (sample MPW-5), and; C_{saline} = the concentration of the constituent in the saline inflow.

Differing water sources mixing within the MNT aquifer where also identified from $^{87}Sr/^{86}Sr$ values including the measurement of a theoretical mixing line predicting the change in the strontium isotopic signature of MNT groundwaters after Faure (1986):

$$\left(^{87}Sr/^{86}Sr\right)_{mix} = \frac{a}{[Sr]} + b \quad (4)$$

where Eq. (4) describes the variation in the $^{87}Sr/^{86}Sr$ value to be expected in a mixture generated by combining various proportions of strontium from two different endmembers with different $^{87}Sr/^{86}Sr$ values. The slope of the line is calculated from Eq. (5):

$$a = [Sr]_A[Sr]_B\left[\left(\frac{\left(^{87}Sr/^{86}Sr\right)_B - \left(^{87}Sr/^{86}Sr\right)_A}{[Sr]_A - [Sr]_B}\right.\right. \quad (5)$$

and the y-intercept from Eq. (6):

$$b = [Sr]_A\left(^{87}Sr/^{86}Sr\right)_A - [Sr]\left(\frac{^{87}Sr/^{86}Sr)_B}{[Sr]_A - [Sr]_B}.\right. \quad (6)$$

These equations require input of the $^{87}Sr/^{86}Sr$ values and [Sr] of endmembers "A" and "B."

Hierarchical cluster analysis (HCA) was performed on log normalised, z-scored data using Unisat 6.0 (UNISTAT, 2011), which supports six similarity measures and ten linkage rules. Similarity measures and linkage rules were varied to identify the distance measure and linkage algorithm that provided the most obvious relationships to geology, hydrochemistry and production well location. As anticipated, the combination of the square of the Euclidean distance (E^2) and Ward's linkage algorithm provided the best interpretability as is often noted by various others applying HCA to groundwater hydrochemical analysis (Daughney et al., 2012; Güler et al., 2002). Field parameters and analytes included in the HCA models were groundwater temperature (°C), pH, SpC, pCO_2, Eh, HCO_3, Cl, SO_4, Na, K, Mg, Ca, Si, S, F, Li, Sr, Ba, Mo and Fe. Removal of Eh and SpC made little difference to the clustering so these were excluded from the final model runs.

4. Results

4.1. Isotopes

The $\delta^{13}C$ values of DIC (or TDC) in Monturaqui groundwaters vary from −2.32 to +0.70‰ (mean = −0.85‰, n = 12) and are significantly more positive (p = ≤0.01) than the average $\delta^{13}C_{DIC}$ values reported for springs (mean = −6.20‰, n = 17), rivers (mean = −5.58‰, n = 7) and groundwaters (mean = −8.24‰, n = 20) throughout northern Chile (Table 1; Fritz et al., 1981; Magaritz et al., 1989). $\delta^{34}S$–SO_4 values range between −0.7 and +4.9‰ with approximately half of the groundwaters having depleted values relative to values reported for regional ground- and spring waters (Risacher and Alonso, 2001; Risacher et al., 2003).

Groundwaters exhibit a narrow range for $\delta^{18}O$ (−8.3 to −7.4‰) and δ^2H (−67.6 to −54.6‰), exhibit a minor trend of ^{18}O depletion (net 1‰) with increasing extraction depth yet show no coherent spatial pattern across the well field. Groundwaters lie to the right of, yet parallel (i.e., s = 8) to the Local Meteoric Water Line (LMWL) defined for modern precipitation in northern Chile: $\delta^2H = 7.8 \cdot \delta^{18}O + 9.7$ (Aravena et al., 1999) along a regional Ground and Spring Water Line (LGSWL; $\delta^2H = 7.99 \cdot \delta^{18}O + 0.3$, n = 95) (Fig. 2). The LGSWL is characterised by a deuterium intercept close to 0‰ and has a $\delta^2H/\delta^{18}O$ value approaching 8 (equilibrium fractionation ratio of Craig (1961)), which is considered an artefact of evaporative enrichment within the snow pack, prior to melt water infiltration, within high altitude recharge zones (Fritz et al., 1981; Magaritz et al., 1989; Peña et al., 1989). Although both $\delta^{18}O$ and δ^2H values of MNT groundwaters are more negative than rainfall collected at the altitude of the MNT aquifer system (Magaritz et al., 1989; Alpers and Whittemore, 1990), it is likely that strong evaporative enrichment of both $\delta^{18}O$ and δ^2H under the high humidity of the snow pack results in an under estimation of the true altitude of recharge (Alpers and Whittemore, 1990; Stichler et al., 2001; Ginot et al., 2006). Enrichment in δ^2H is evident in the brackish groundwaters from well MPW-9, which contain a measured deuterium excess (d-excess) of ~7‰, is likely due to hydrogen exchange with lacustrine clays during basal leakage of evaporitic brines.

Strontium isotope ($^{87}Sr/^{86}Sr$) values range between 0.706859 and 0.707348 for the 7 samples measured and span the range of values reported for the Negrillar Volcanics andesite, Socompa lavas and coeval ignimbrites (Déruelle and Moorbath, 1993; Mamani et al., 2008).

4.2. Chemical modelling

Modelled pCO_2 values (Eq. (2)) are anomalously high, 0.016 to 0.10 atm or ~50–316 times atmospheric values (Fetter, 1994; Clark and Fritz, 1997). Saturation indices indicate that all but one of the groundwaters, well MPW-19, are theoretically saturated to over saturated with respect to carbonate minerals (calcite and aragonite) (Table 5). Anhydrite and gypsum are both theoretically under saturated in all groundwater samples although the saturation index approaches a value of −1.0 and −0.9, respectively in the duplicate samples from well MPW-9. All samples are close to equilibrium (±0.5) with respect to cristobalite (volcanic glass) and other cryptocrystalline amorphous forms of silica (chalcedony) but strongly under saturated with respect

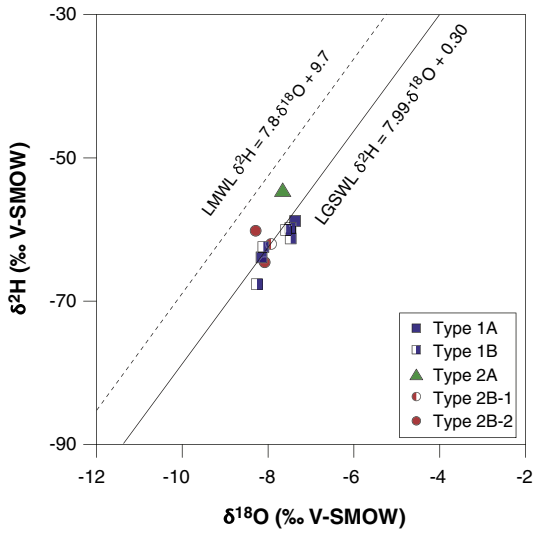

Fig. 2. Plot of $\delta^{18}O$ vs $\delta^{2}H$ for MNT groundwaters. Also shown: the Local Meteoric Water Line (LMWL) for the South Central Andes from Aravena et al. (1999); the Local Ground- and Spring-Water Line (LGSWL) for the South Central Andes based on data (n = 95) from Fritz et al. (1981), Magaritz et al. (1989), Aravena and Suzuki (1990) and Alpers and Whittemore (1990).

to halite and other highly soluble salts (e.g., antarcticite; $CaCl_2 \cdot 6H_2O$). Approximately half of the groundwaters sampled are close to saturation with respect to barite, four are slightly over saturated and six slightly under saturated. All samples are under saturated with respect to celestite ($SrSO_4$) but over saturated, with the exception of groundwaters from well MPW-19, with respect to strontianite.

4.3. Hierarchal cluster analysis

At the scale of lowest resolution the dendrogram of MNT groundwaters identifies two clusters of groundwaters that are significantly different (Fig. 3; Tables 2–4). Type 1 groundwaters account for 58% of the wells sampled and all intersect, or are partially screened, within the Negrillar Volcanics, distal from Volcano Socompa. Type 2 groundwaters represent the remaining 42% of wells sampled and represent groundwaters south of the Negrillar Volcanics and proximal to Volcano Socompa. Type 1 groundwaters have lower TDS concentrations (incl. Na, Cl, Ca and SO_4), lower and more reducing Eh values, lower temperatures and pCO_2 but slightly higher pH and significantly higher dissolved Fe and Mn concentrations compared to Type 2 groundwaters. At the major ion level, Type 1 groundwaters are Na–(Ca)–HCO_3 waters whereas for Type 2 waters, Na is the dominant cation and major anion dominance varies between Cl, HCO_3 and SO_4.

At the 100-phenon line Type 2 groundwaters are resolved into two further subclusters, 2A and 2B. Type 2B groundwaters constitute 35% of the groundwaters sampled and represent the subset of wells occurring closest to Volcano Socompa. Type 2A groundwaters, although genetically related at the major level to Type 2 water, are chemically distinct at the 100-phenon line from all other waters and are restricted to the duplicate samples drawn from well MPW-9. Type 2A groundwaters contain approximately twice the TDS of all other groundwaters sampled, are the only waters with Na–(Ca)–Cl–(SO_4) facies and the most oxidising (Eh = +150 mV) groundwaters sampled within the MNT system (Fig. 1).

At the highest resolution, the 50 phenon line, 5 distinct subclusters of MNT groundwaters are identified (Fig. 3). Types 1A and 1B constitute 23 and 35% of the groundwaters sampled, respectively whereas subclusters 2B-1 and 2B-2 constitute between 12 and 24%, respectively. Types 1A and 1B are broadly similar and both are associated with the Negrillar Volcanics. However, Type 1A groundwaters contain the lowest TDS of waters sampled within the MNT aquifer system and are differentiated from Type 1B groundwaters by lower major ion and dissolved Fe concentrations.

Groundwater Types 2B-1 and 2B-2 both occur within the southern Monturaqui portion of the aquifer system. Type 2B-1 groundwaters (wells MPW-14 and MPW15) occur directly south of the Negrillar Volcanics and are screened at slightly greater depths (ca. 20–40 m deeper) than the rest of the wells sampled. Deeper Type 2B-1 groundwaters are strongly reduced (lowest Eh), Na–HCO_3 groundwaters, of elevated pCO_2 and the highest concentration of non-SO_4 sulfur as well as being some of the few groundwaters over saturated with respect to barite. Type 2B-2 groundwaters associated with the southernmost cluster of wells (MPW-17 to MPW-20) are screened at relatively shallow depths similar to that of well MPW-9 (Type 2A waters) and are genetically most similar to Type 2A waters.

4.4. Physiochemical parameters

Groundwater temperatures range from 27 °C to 37 °C and TDS from 826 to 3632 mg l^{-1} (Tables 2 - 4). The majority of groundwaters are neutral to alkaline (pH = 6.8–7.9) and, with the exception of well MPW-9 (Eh = +150 mV), are reducing (Eh = −27 to −170 mV). Bicarbonate is the most common anion followed by Cl and SO_4, and Na is the most abundant cation followed by Ca. Relative to regional norms, groundwater DIC and SiO_2 concentrations are elevated (Fritz et al., 1981; Magaritz et al., 1989). The odour of H_2S was evident in a number of northern wells within the Negrillar Volcanics.

Table 5
Theoretical mineral saturation indices (log Q/K) modelled for MNT groundwaters.

Well	Cluster	Antarcticite	Halite	Anhydrite	Calcite	Aragonite	Chalcedony	Cristobalite	Dolomite	Gypsum	Barite	Siderite	Celestite	Strontianite	Witherite
MPW-11	1A	−12.5	−6.7	−1.9	0.1	0.0	0.6	0.3	1.1	−1.8	−0.1	−1.6	−2.4	0.3	1.0
MPW-21	1A	−12.4	−6.7	−1.8	0.6	0.4	0.5	0.3	1.9	−1.7	−0.1	0.6	−2.4	0.7	1.4
MPW-5	1A	−12.5	−6.8	−1.9	1.0	0.9	0.5	0.2	2.8	−1.8	−0.2	−1.4	−2.3	1.3	1.8
MPW-8	1A	−12.4	−6.7	−1.8	0.7	0.5	0.5	0.3	2.1	−1.7	0.1	−0.8	−2.4	0.8	1.7
MPW-10	1B	−12.8	−6.8	−1.4	1.0	0.8	0.5	0.3	2.8	−1.3	−0.2	0.2	−2.2	0.8	1.2
MPW-13	1B	−11.9	−6.4	−1.6	0.8	0.7	0.5	0.3	2.3	−1.5	−0.3	0.7	−2.2	0.9	1.2
MPW-2	1B	−11.5	−6.1	−1.6	0.9	0.7	0.6	0.3	2.5	−1.4	−0.2	−1.5	−2.0	1.1	1.3
MPW-3	1B	−11.8	−6.3	−1.8	1.0	0.8	0.6	0.3	2.8	−1.6	−0.1	0.9	−2.3	1.1	1.7
MPW-4	1B	−12.2	−6.6	−1.7	1.0	0.8	0.5	0.2	2.5	−1.5	−0.3	0.6	−2.3	1.0	1.4
MPW-7	1B	−11.5	−6.1	−1.5	0.9	0.8	0.5	0.3	2.7	−1.4	−0.5	1.4	−2.0	1.1	1.0
MPW-9	2A	−10.0	−4.7	−1.0	0.9	0.8	0.6	0.3	2.8	−0.9	0.0	−1.1	−1.2	1.4	1.1
MPW-14	2B-1	−11.6	−6.1	−1.4	0.9	0.7	0.5	0.2	2.6	−1.3	0.3	−0.9	−1.9	1.0	1.6
MPW-15	2B-1	−11.2	−5.9	−1.4	0.8	0.6	0.5	0.3	2.5	−1.2	−0.3	−0.9	−1.7	1.0	0.9
MPW-17	2B-2	−11.6	−6.0	−1.2	0.2	0.0	0.6	0.3	1.3	−1.1	0.3	−1.5	−1.7	0.3	0.7
MPW-18	2B-2	−11.2	−5.5	−1.3	0.6	0.4	0.5	0.2	2.1	−1.2	0.4	−1.3	−1.7	0.7	1.3
MPW-19	2B-2	−11.7	−6.1	−1.2	−0.1	−0.3	0.5	0.3	0.7	−1.1	0.1	−2.1	−1.7	−0.1	0.2
MPW-20	2B-2	−11.2	−5.6	−1.3	0.6	0.4	0.5	0.3	2.1	−1.2	−0.1	−1.1	−1.8	0.7	0.8

Mineral saturation indices (log Q/K) modelled for MNT groundwaters. Where (−) negative values reflect undersaturation, positive values oversaturation, and 0 indicates equilibrium.

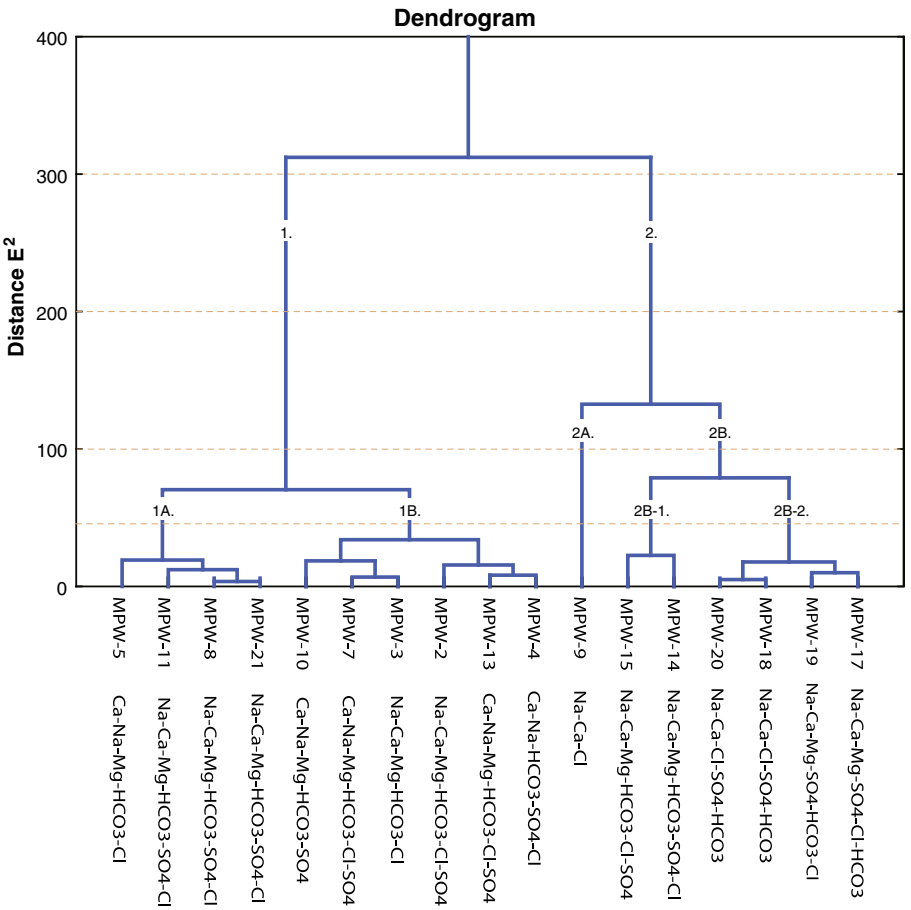

Fig. 3. Dendrogram for MNT groundwater wells using (°C), pH, pCO_2, HCO_3, Cl, SO_4, Na, K, Mg, Ca, Si, S, F, Li, Sr, Ba, Mo and Fe and Ward's linkage rule with the square of the Euclidean distance (E^2) as the similarity measure. Water type expressions provided for each groundwater are based on milliequivalent percentage values and is formed by listing the ions with concentrations greater than 10% in decreasing order (cations are listed first).

Following the criteria of Drever (1997), MNT groundwaters fall close to the threshold between fresh (<1000 mg l^{-1}) and brackish (1000–20,000 mg l^{-1}) groundwaters (Tables 2–4). Of the 17 groundwaters sampled, seven exceed a TDS of 1500 mg l^{-1} with only well MPW-9 exceeding 2000 mg l^{-1}. The median TDS load of Type 2B groundwaters is 30% higher than the median of Type 1 (Negrillar) groundwaters. The brackish groundwater from well MPW-9 (Type 2A) contains approximately 2–4 times the salt load of all other groundwaters. Of the waters sampled, well MPW-5 has the lowest TDS concentration, 826 mg l^{-1}, and is the only groundwater for which SO_4 is not a major ion (<10% on a milliequivalent basis). The TDS concentration for well MPW-5 is closest to the theoretical TDS load (600 mg l^{-1}) modelled for purely meteoric dissolution of average volcanic rock compositions for the South Central Andes (Risacher and Fritz, 2008; Risacher et al., 2011). From the work of Risacher et al. (2003, 2011), all MNT groundwaters fall well below the 5000 mg l^{-1} threshold designated for dilute inflow waters across the region.

5. Discussion

All groundwaters sampled from the MNT aquifer system are classified as thermal waters based on a minimum temperature difference of ~20.4 °C between the coolest groundwater (26.5 °C) sampled and the mean annual air temperature of the MNT trough (~6.1 °C). A maximum difference of 28.5 °C was recorded for the groundwaters extracted from well MPW-18 proximal to Volcano Socompa.

5.1. Spatial patterns and solute sources

Plots of temperature (°C) and pCO_2 display a relatively uniform increase with increasing proximity to the summit of Volcano Socompa, indicative of an increasing vapour phase flux of steam and CO_2 boiled off an underlying volcanic-hydrothermal reservoir (Fig. 4). Although wells MPW-5 and 7 depart from the general trend, probably due to sheltering by low permeability vents and dykes of the El Negrillar Volcanics, groundwater temperature and pCO_2 increases from 26.5 °C to 34.5 °C and 0.02–0.1 atm, respectively. The theoretical equilibrium $\delta^{13}C$–CO_2 signature of the original CO_2 source dissolving within MNT groundwaters, computed using Eq. (2), ranges from −9.25‰ to −3.55‰ falling within the range typically reported for subduction zone CO_2 (i.e., −10.0 to −3.5‰ $\delta^{13}C$) (Fischer et al., 1998; Lewicki et al., 2000). Modelled values are also similar to the range of $\delta^{13}C$–CO_2 (−0.60‰ to −9.00‰) reported for thermal springs and CO_2 sources from the Central Andean Volcanic Arc (Spiro et al., 1997) and volcanic hydrothermal systems of northern Chile (Capaccioni et al., 2011). The fraction of isotopically enriched $\delta^{13}C$–CO_2 increases in conjunction with the pCO_2 (mass flux) as the wells get closer to Volcano Socompa, approaching values typical of the mantle ($\delta^{13}C = -4.0 \pm 2.5$‰; Fig. 5; Hards, 2005).

Despite being similar to atmospheric values, the isotopically lighter $\delta^{13}C$–CO_2 signatures occurring in Type 1A groundwaters within the Negrillar Volcanics have modelled pCO_2 and DIC concentrations (>5 mmol/l) that are much too high to be explained by open system exchange with atmospheric or desert zone soil CO_2 (Drever, 1997; Rech

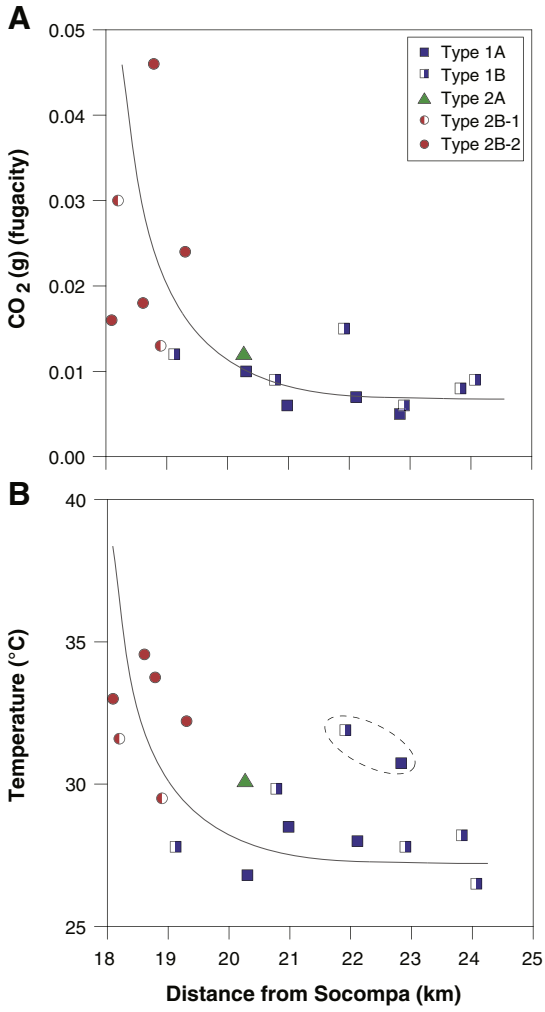

Fig. 4. Pattern of increasing (A) CO_2 fugacity and (B) groundwater temperature with proximity to the summit of Volcano Socompa. Note the generally smooth exponential increase in pCO_2 and temperature with proximity to the summit as is consistent with the: (i) greater mobility of vapour phase constituents; (ii) the adsorption of steam and CO_2, boiled off a deep hydrothermal reservoir, within the cool meteoric groundwaters of the MNT aquifer, and; (iii) an increase in mass and heat flow with proximity to the major upflow zone of a deep hydrothermal reservoir associated with Volcano Socompa. Dashed oval encompasses wells MPW-5 and 7 that depart from the general trend, probably due to sheltering by low permeability vents and dykes of the El Negrillar Volcanics, which exclude cooler recharge waters from the east.

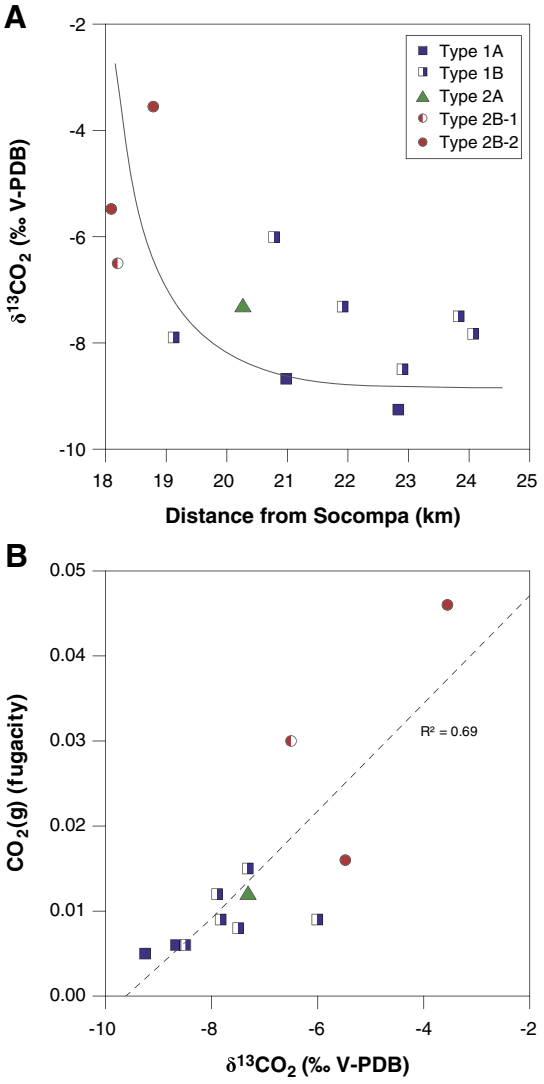

Fig. 5. (A) $\delta^{13}C$–CO_2 displays an increasingly magmatic signature with proximity to the summit of Volcano Socompa. (B) Moderate/strong correlation between $\delta^{13}C$–CO_2 and CO_2 mass flow (pCO_2 fugacity). Both relationships highlight the increasing heat and mass flow with proximity to major upflow zone of a deep hydrothermal reservoir associated with Volcano Socompa.

et al., 2003; Leybourne et al., 2013). Pedogenic carbonates from a transect through a portion of the MNT aquifer system and the flanks of Volcano Socompa all have $\delta^{13}C$–CO_2 values suggestive of partial equilibrium with atmospheric CO_2 and are much too enriched to have originated from respiration of isotopically depleted (C3-cycle, ca. −23‰) organic matter (Quade et al., 2007). This observation is consistent with the hyperarid setting of the Atacama desert and indicates that soil zone partial pressures seldom exceed atmospheric values and that unlike more humid environments soil organic carbon likely plays a minimal role in alkalinity generation during recharge. Furthermore, because isotopically enriched marine carbonates are largely absent from the Andean arc (Spiro et al., 1997), the $\delta^{13}C$–CO_2 values and anomalous DIC concentrations of MNT groundwaters are best explained by the typical $\delta^{13}C$–CO_2 range of subduction zone settings, albeit trending towards more mantle-like values with increasing proximity to Volcano Socompa.

Whereas groundwater temperature, pCO_2 and $\delta^{13}C$–CO_2 display a relatively uniform increase with proximity to the summit of Volcano Socompa the majority of ions do not. Chloride, SO_4, Na, K, Mg, Sr, Li, F, Cu, Mo, As, Zn, V and Cs all show a sharp structurally controlled increase south of Negrillar and are most elevated within Type 2A (MPW-9) groundwaters (Fig. 6). This distinct structural partitioning is interpreted as a transition from predominately vapour phase-derived solute supply within the Negrillar Volcanics (Type 1 waters) to a combination of secondary hydrothermal vapour phase and liquid phase solute supply within the Monturaqui portion (Type 2 waters) of the system (Fig. 7). In this instance, sheltering by low permeability dykes and vents within the Negrillar Volcanics, appears to restrict the mixing of the liquid phase solute outflow. Transition metal concentrations, especially Fe and Mn, appear to be spatially controlled by redox state (Fig. 8).

Strontium isotope values also support a shift in solute sources and source mechanisms inside and outside of the Negrillar Volcanics (Fig. 9). The $^{87}Sr/^{86}Sr$ values for Type 1 groundwaters within the Negrillar Volcanics, 0.707198–0.707375, fall within the andesite range (0.707–0.708) reported for these rocks (Déruelle and Moorbath, 1993) and, in conjunction with the hydrochemical facies (Na–(Ca)–HCO_3), supports the concept of dominantly localised gas–water–rock interaction between the Negrillar Volcanics and a hydrothermal vapour phase.

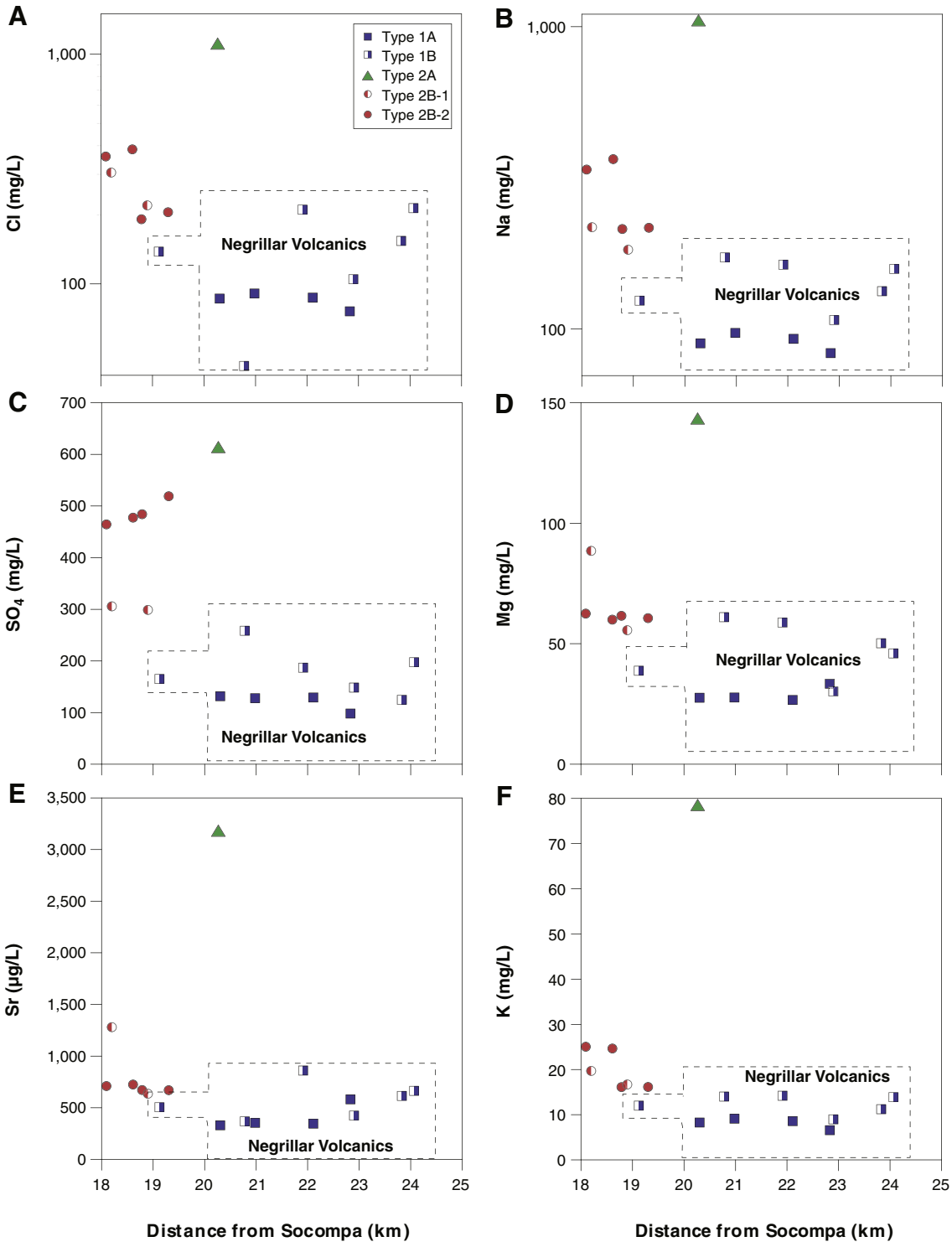

Fig. 6. (A–F) Evidence of structural control over solute sources. Note the abrupt increase in solutes outside of the Negrillar Volcanics that reflects the role of localised dykes and sills in blocking liquid phase lateral inflows containing elevated solute concentrations originating from the east. Dashed box encompasses all wells that transect the lavas of the Negrillar Volcanics.

Type 2A groundwater from well MPW-9 has ca. 7 times the Sr concentration of other groundwaters within the MNT aquifer system and the least radiogenic $^{87}Sr/^{86}Sr$ value, 0.70685, of the data set. This value is close to the median $^{87}Sr/^{86}Sr$ value reported for Socompa lavas (0.70681) by Mamani et al. (2008) and is within the range of values reported for andesite and dacite lava from young Andean stratovolcanoes and ignimbrites of the South Central Andes, including the Salín Formation (e.g., 0.705–0.707; Déruelle and Moorbath, 1993; Kraemer et al., 1996).

Despite the overlap of $^{87}Sr/^{86}Sr$ with local Salín Formation ignimbrites it is difficult to attribute the abrupt increase in the non-volatile solute load of Type 2 groundwaters to secondary gas–water–rock interaction between the Salín Formation and a hydrothermal vapour phase. Rather, a solute source with high Sr concentrations and $^{87}Sr/^{86}Sr$

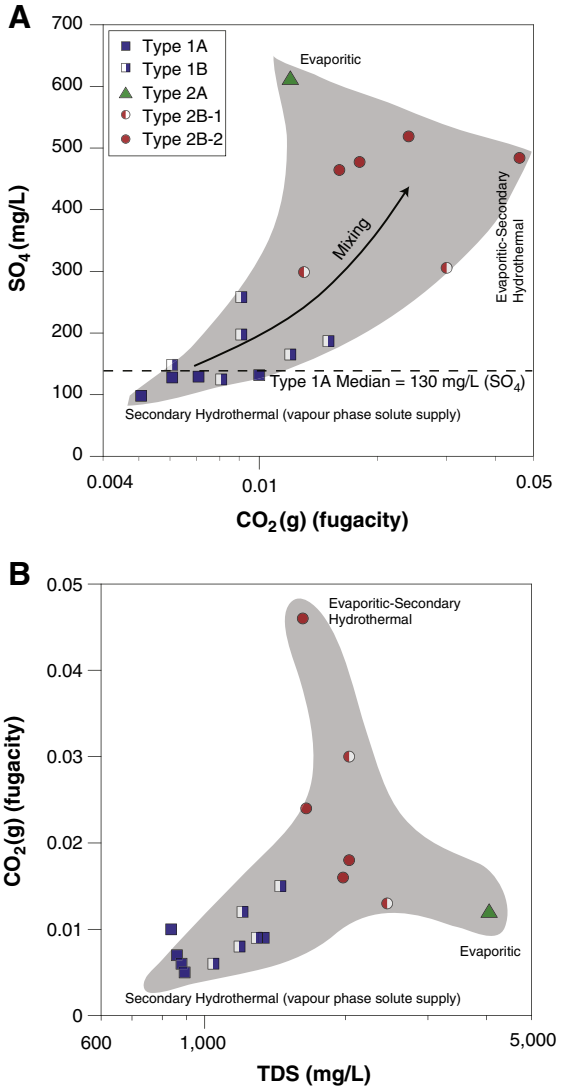

Fig. 7. Vapour phase versus liquid phase solute supply within the MNT aquifer system. (A) Sulfate mixing dynamics. Note mixing between low sulfate, secondary hydrothermal groundwaters and high SO_4 groundwaters associated with evaporitic inputs. (B) Relationship of pCO_2 and TDS reflecting the departure from predominantly secondary-hydrothermal solute supply to dominantly evaporitic and mixed evaporitic-hydrothermal. It is difficult to account for the strong increase in non-volatile species by purely hydrothermal gas–water–rock interaction with low Cl host rocks suggesting a second solute source associated with lateral inflows from the east.

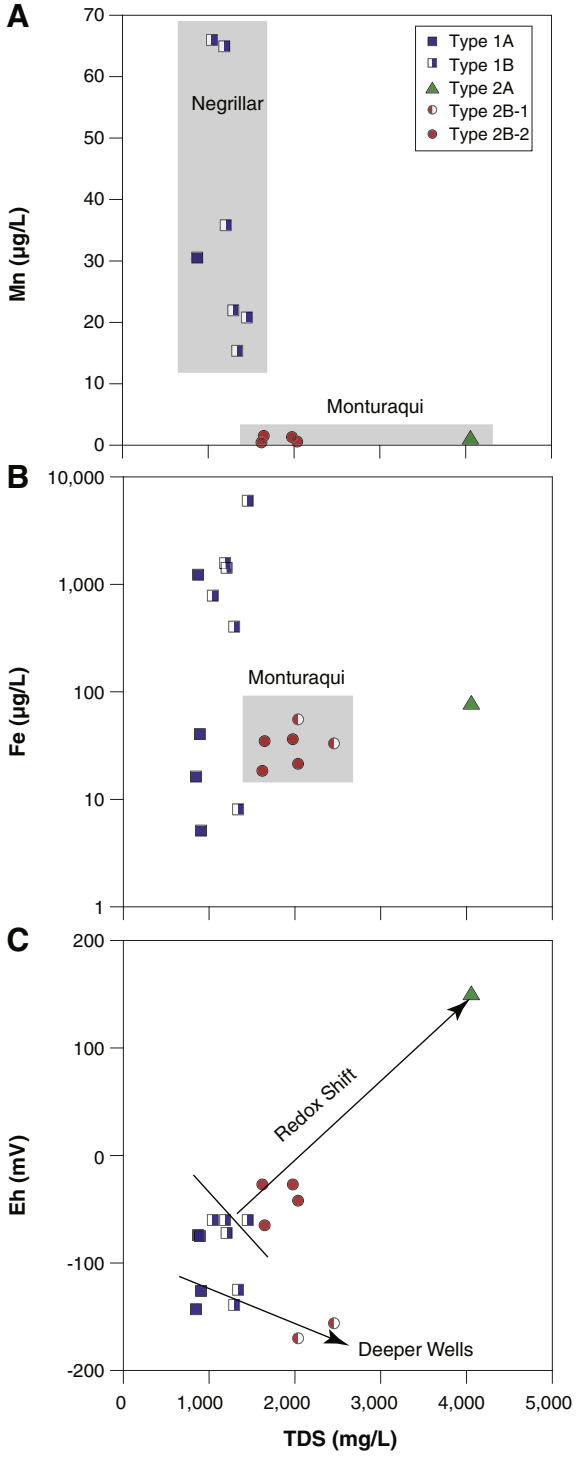

Fig. 8. (A–B) Structural controls over dominant fluid compositions and resultant trends in redox sensitive transition elements Fe and Mn. Fe^{II} and Mn^{II} concentrations are elevated in Type 1 groundwaters within the Negrillar Volcanics where inputs of reduced hydrothermal gases dominate. Conversely, groundwaters outside of the sheltered Negrillar Volcanics contain minimal reduced Fe^{II} and Mn^{II} reflecting a shift in redox state due to mixing with a strongly oxidising evaporitic brine. During brine evolution in shallow oxidised salars Fe and Mn precipitate as oxides and do not infiltrate to depth (Herrera et al., 2009) (C). Redox shift caused by mixing of reduced secondary hydrothermal groundwaters with oxidising evaporitic waters. As well depth increases the relative proportion of reduced hydrothermal fluids increases as seen in wells MPW-14 and MPW-15.

signatures similar to those of Socompa lavas is indicated. Type 2B groundwaters demonstrate intermediate $^{87}Sr/^{86}Sr$ values dominated by lesser radiogenic signatures similar to brackish Type 2A waters of well MPW-9, suggesting varying degrees of mixing between Sr derived from localised gas–water–rock interaction and Sr derived from mixing with Type 2A brackish waters (Fig. 10).

Sulfur isotopes ($\delta^{34}S$–SO_4) also suggest a structurally controlled shift in solute sources and source mechanisms inside and outside of the Negrillar Volcanics (Fig. 9). The $\delta^{34}S$–SO_4 signature of Type 1 groundwaters within the Negrillar Volcanics is significantly lower than $\delta^{34}S$–SO_4 signatures for continental gypsum (+3 to +11‰; Spiro and Chong, 1996; Risacher and Alonso, 2001) and surface waters (+3.4 to +7.4‰) reported for the South Central Andes (Fig. 9). Rather, the $\delta^{34}S$ values determined for SO_4 in Type 1 Negrillar groundwaters (+0.8 to +2.3; median = 1.8‰), are similar to values reported for dissolved SO_4 from H_2S-rich, steam heated thermal waters from around the world (i.e., −1.7 to +1.4‰; Schoen and Rye, 1970).

In shallow meteoric groundwaters subject to vapour phase inputs of steam and hydrothermal gases (CO_2 and H_2S), SO_4 is typically derived from meteoric oxidation of hydrothermal H_2S (Marini et al., 2000;

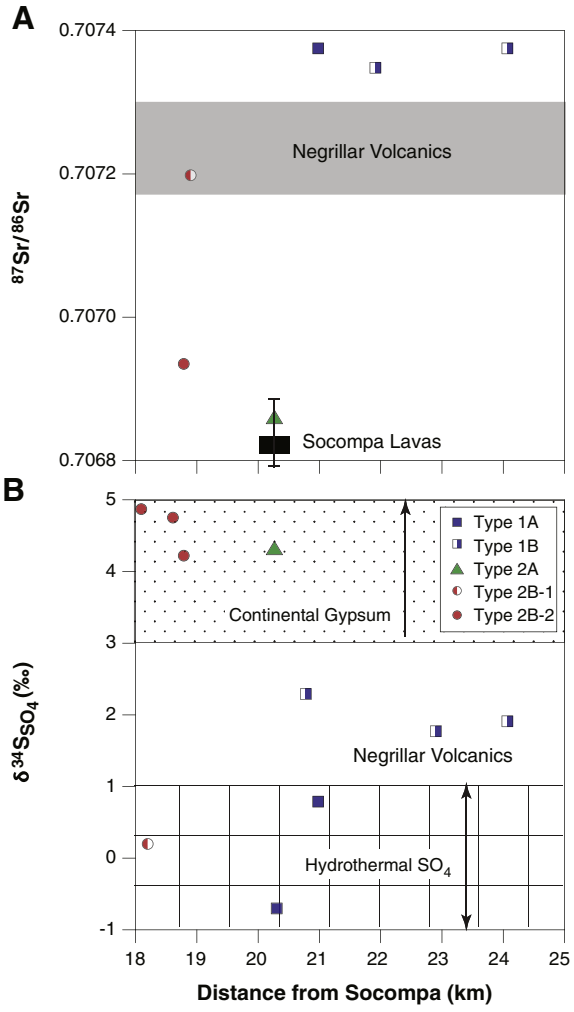

Fig. 9. Structural partitioning and evidence for two distinct solute sources as defined by $^{87}Sr/^{86}Sr$ values and $\delta^{34}S$–SO_4 for the groundwaters of the MNT aquifer system. (A) Groundwaters within the Negrillar Volcanics show a localised Sr source signature supportive of gas–water–rock interaction between Negrillar rocks and secondary hydrothermal fluids boiled of a deep hydrothermal reservoir. Groundwaters (Type 2) within the Monturaqui portion of the aquifer system contain up to ca. 7 times the Sr concentration of groundwaters within the MNT aquifer system and have $^{87}Sr/^{86}Sr$ values that are similar to Socompa lavas and the ignimbrites and lavas of the Andean volcanic arc. (B) $\delta^{34}S$–SO_4 values transition from dominantly hydrothermal $\delta^{34}S$–SO_4 signatures within Type 1 (Negrillar) groundwaters to continental gypsum signatures within Type 2 (Monturaqui) groundwaters raising the possibility of an evaporitic origin for the excess salts within the latter.

Marini and Gambardella, 2005). Volcanic-hydrothermal H_2S typically has a value close to 0‰ relative to V-CDT, consistent with a primary mantle sulfur source (Krouse, 1976; Clark and Fritz, 1997). Oxidation of hydrothermal H_2S to SO_4 is typically a non-equilibrium, low-temperature process that involves a small (~1‰) enrichment in the SO_4 phase producing isotopic signatures that range from −1 to +1‰ (±2‰) (Krouse, 1974; Kiyosu and Kurahashi, 1983; Clark and Fritz, 1997).

Although a volcanic-hydrothermal origin is apparent for the bulk of the SO_4 occurring within Type 1 (Negrillar Volcanics) groundwaters, meteoric oxidation of hydrothermal H_2S cannot however, produce the heavier $\delta^{34}S$–SO_4 (i.e., +4.2 to +4.9‰) values of dissolved SO_4 found in Type 2 groundwaters. These heavier $\delta^{34}S$–SO_4 values overlap with gypsum/anhydrite signatures found in actively forming evaporitic lakes (+4.0 to +9.0‰) (Risacher and Fritz, 1991; Pueyo et al., 2001; Risacher and Alonso, 2001) and those for SO_4 derived from the disproportionation of magmatic SO_2 under moderate to high temperatures (≥200 °C) within the volcanic plumbing system of Andean volcanoes (Kusakabe et al., 2000).

Based on all of the above, the question arises as to whether the saline liquid phase input best characterised by Type 2A groundwaters (well MPW-9) is derived from an alkali-Cl outflow associated with a convecting hydrothermal system beneath Volcano Socompa or the inflow of basinal evaporitic brines. Both are feasible, however, on the basis of chemistry alone the liquid phase solute profile evident within the Monturaqui section of the aquifer system (MPW-9 especially) appears remarkably similar to that of the sulfate neutral evaporitic brines (Na–SO_4–Cl) typical of the Andean volcanic arc and high altiplano (see Risacher et al., 2003; Risacher and Fritz, 2008).

5.2. Mixing proportions

Using Eq. (3), the waters from well MPW-5 as the meteoric end member and MPW-9 as the saline endmember the proportions of Cl (median) derived from the evaporitic component in well MPW-9 are estimated at 1% (within error) for Type 1A waters, 11% for Type 1B, increasing to 23 and 27% for Types 2B-1 and 2B-2, respectively (Fig. 10). Wells MPW-18 and MPW-20 (Type 2B-2) show the greatest component, up to ~40%, of the evaporitic component from well MPW-9 (Type 2A). Application of Eq. (3) to Na, K and Li also indicate similar mixing proportions to those obtained using Cl. The mixing proportions obtained from simple two component mixing equations approximate those inferred from multivariate statistics, using the Euclidean distance as a measure of similarity, and $^{87}Sr/^{86}Sr$ isotope values and Sr concentration (Eqs. (3)–(6); Fig. 10).

5.3. Physical and chemical composition of evaporitic component

A more complete, albeit approximate, picture of the chemical composition of the evaporitic brine evident in Type 2A (MPW-9) groundwaters is produced by subtracting the secondary hydrothermal component most evident in Type 1A waters from mixed Type 2A waters that contain the greatest evaporitic component. Subtraction removes almost all of the alkalinity and Si suggesting that these species are derived from localised gas–water–rock interaction and that little if any alkalinity or Si is associated with the evaporitic component (see Section 5.2).

The depletion in alkalinity and Si may be explained in terms of evaporitic brine evolution. Specifically, depletion in alkalinity reflects removal during calcite precipitation from low alkalinity inflows typical of the Andean arc, reducing significantly the proportion of CO_3 within the residual liquid (Risacher and Fritz, 2008). Similarly, the biogenic precipitation of amorphous silica within evaporitic lakes is a common and highly effective mechanism removing Si from solution (DeMaster, 2004; Deocampo, 2005).

Because the majority of silica is associated with local gas–water–rock interaction and silica behaves in a *relatively* conservative manner at the low temperatures and pH values (≤8.0) of the MNT aquifer (i.e., dissolved Si does not behave like a charged ion or colloid; Hem, 1985), the enrichment of various species within the evaporitic component can be approximated by:

$$EF = \left(X_{(2A)}/Si_{(2A)}\right) / \left(X_{(1A)}/Si_{(1A)}\right) \quad (7)$$

where EF is the enrichment factor for the chemical species of interest, X is the concentration of the given species, Si is the concentration of silica, and subscripts 2A and 1A denote the concentration of chemical species in Type 2A evaporitic waters and the median value of Type 1A secondary hydrothermal waters, respectively. From Eq. (7) the general enrichment pattern for major ions follows the pattern Cl (~10), Na (~9), K (~8), SO_4 and Mg (~4), and Ca (~3); minor alkali and alkali earth metals Cs (~20), Li (~10), Sr (~7) and Rb (~3), and; trace components Mo (~31), Re (~18), As (~14), Al (~13), V (~7), Zn (~6), F (~5), Se (~4)

A) Two component mixing (%)

Well Name	Cluster	F_{saline}(Cl)	F_{saline}(Na)	F_{saline}(K)	F_{saline}(Li)
MPW-5	1A	0	0	0	0
MPW-11	1A	1.0	0.7	2.4	1.2
MPW-21	1A	1.1	1.0	2.9	2.0
MPW-8	1A	1.5	1.5	3.7	2.0
Median		1.1	1.0	2.9	2.0
MPW-4	1B	2.9	2.6	3.4	3.3
MPW-13	1B	6.5	4.5	8.2	5.9
MPW-3	1B	8.2	5.5	6.9	7.8
MPW-10	1B	13.4	10.3	11.6	12.9
MPW-7	1B	15.2	9.1	11.9	13.0
MPW-2	1B	15.6	8.5	11.4	10.6
Median		10.8	7.0	9.8	9.2
MPW-14	2B-1	16.3	11.6	16.4	22.9
MPW-15	2B-1	28.9	16.3	22.4	22.2
Median		22.6	14.0	19.4	22.6
MPW-17	2B-2	14.4	16.1	15.4	21.5
MPW-19(b)	2B-2	12.7	15.8	15.3	21.8
MPW-20	2B-2	38.2	36.0	34.7	45.1
MPW-18	2B-2	43.3	41.7	33.7	46.3
Median		26.3	26.1	24.5	33.4
MPW-9	2A	100	100	100	100

B) Degree of similarity

Sample	Cluster	Corr Coeff	Euclidean distance	Nº Analytes
MPW-5	1A	1.00	0	4
MPW-11	1A	1.00	12	4
MPW-21	1A	1.00	15	4
MPW-8	1A	1.00	20	4
MPW-4	1B	1.00	38	4
MPW-13	1B	0.99	75	4
MPW-3	1B	0.99	93	4
MPW-7	1B	0.97	157	4
MPW-2	1B	0.96	157	4
MPW-14	2B-1	0.98	175	4
MPW-15	2B-1	0.95	266	4
MPW-17	2B-2	1.00	186	4
MPW-19(b)	2B-2	1.00	175	4
MPW-20	2B-2	0.99	380	4
MPW-18	2B-2	0.99	419	4
MPW-9	2A	0.99	1403	4

Used Parameters Na,Cl,K,Li
Main Sample: MPW-5

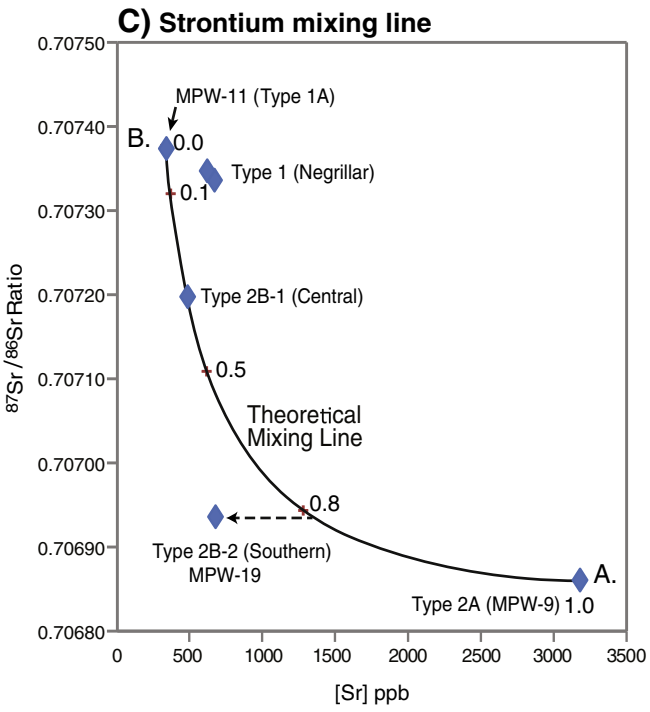

Fig. 10. Secondary hydrothermal and evaporitic mixing relationships for MNT groundwaters. (A) Two component mixing where the fraction of saline evaporitic input (F_{saline}) is calculated for individual samples according to major ions (dominantly conservative species), expressed as a %. (B) Euclidian measure of similarity based on the same major ions that show a similar pattern to that expressed by two component mixing. Groundwaters most dissimilar from the MPW-5 (Type 1A endmember) coincide with those that contain the greatest evaporitic component and all lie outside the Negrillar Volcanics. (C) Strontium chemistry of MNT groundwaters formulas after Faure (1986). This model demonstrates mixing between various proportions of Sr from Sr poor groundwaters (Type 1A) within the Negrillar Volcanics (endmember B) and Sr rich groundwaters within the evaporite containing groundwaters of well MPW-9 (endmember A). The weight fraction of endmember A in the two-component mixture is indicated along the mixing line. The selection of each respective endmember is based on evidence for two distinct Sr sources mixing within the MNT aquifer system: (i) Sr derived from localised secondary hydrothermal water rock interaction (Type 1A; MPW-5 endmember), and; (ii) Sr imported within the evaporitic component most evident in well MPW-9 (endmember A). For the most part, samples fall along or close to the theoretical mixing line between both endmembers supporting the two component mixing model proposed within the text, although a clear deviation of Type 2B-2 groundwaters from the mixing line is apparent (dashed arrow). Deviation from the mixing line for well MPW-19 reflects dilution of the Sr concentration by a significant secondary hydrothermal component within this groundwater as is evident in Figs. 4, 5 and 7.

and Cr (~2). Manganese, Fe, Co, Ni and Cu are not enriched in the evaporitic phase relative to Type 1A waters.

Enrichment of Mo, Re, As, V and Se suggests a source environment characterised by oxidising alkaline conditions, which favours the formation of highly soluble oxyanions (Garrels and Christ, 1965; Hem, 1985; Masscheleyn et al., 1991; Banks et al., 2004; Oremland et al., 2004; Leybourne and Cameron, 2008; Hamamura et al., 2012). Whereas Mo (probably as MoO_4^{2-}), Re (ReO_4^-), As ($HAsO_4^{2-}$), V ($H_2VO_4^-$ or HVO_4^{2-}), Se (SeO_3^{2-} or SeO_4^{2-}) and Cr (CrO_4^{2-}) all form soluble oxyanions under oxidising alkaline conditions, Mn, Fe, Co, Ni and Cu form insoluble precipitates or co-precipitate with iron and manganese oxides and are removed from solution (Hem, 1985; Banks et al., 2004; Morford et al., 2005; Leybourne and Cameron, 2008).

Enrichment of Fe, Mn, Co, Ni and Cu within solid phase carbonates and relatively depleted concentrations of the more soluble oxyanion species is reflected in sediments from evaporitic lakes within the altiplano and significantly is the inverse of the enrichment pattern evident in Type 2A waters (Fig. 11; Herrera et al., 2009). (Although As is also enriched in the sediments of high altitude salars (Herrera et al., 2009), high concentrations (up to 32 mg l^{-1} As) are reported for the liquid

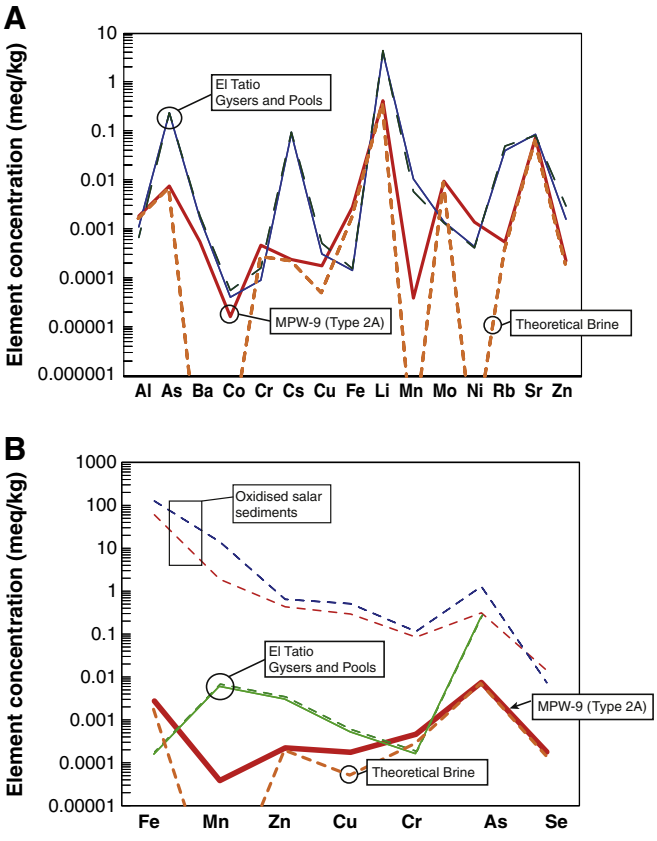

Fig. 11. Schoeller diagrams demonstrating the different solute profiles of evaporite containing MPW-9 (Type 2A) groundwaters, theoretical brine composition, high temperature hydrothermal fluids (El Tatio; Cortecci et al., 2005) and lagoon sediments of the Huasco and Coposa salars (Herrera et al., 2009). (A) Pronounced differences between the chemical composition of Type 2A, theoretical evaporitic brine composition (see Section 5.4.) and high temperature hydrothermal fluids from El Tatio reflect the contrasting physiochemical settings — brine evolution within an oxidising, alkaline evaporitic lake versus high temperature hydrothermal reservoir. Here differences reflect the dominant controls of temperature and redox state over mineral solubility, in particular Ba, Co, Mn and Ni. (B) Relative abundance of Fe, Mn, Zn, Cu, Cr, As and Se for oxidising salar sediments relative to evaporite containing MPW-9 groundwaters (Type 2A) and theoretical evaporitic brine (see Section 5.4). In oxidised salar sediments Fe(III) and Mn(IV) predominate whereas in reduced hydrothermal waters Fe(II) and Mn(II) predominate. Conservative oxyanions of As and Se show a similar profile for salar sediments and MPW-9 waters and that of the theoretical brine composition. The difference between ion speciation and abundance is again a factor of the dominant controls of temperature, ionic strength and redox state over mineral solubility.

phase within salars of the hyperarid Central Andes (Farias et al., 2011)). Additionally, the trace element enrichment patterns within alkali-Cl waters of the El Tatio geothermal field are distinctly different to those of the evaporitic component most evident in Type 2A groundwaters reflecting the lower pH (~5.8) and reducing conditions (mean Eh = −254 mV based on redox pairs $S(^{-}2)/S(^{+}6)$) (Cortecci et al., 2005), of these high temperature fluids (Fig. 11).

The strongly oxidising environment for the evaporitic brine, inferred from trace element enrichment patterns, is supported by measured redox potentials of +150 mV (O_2-reducing) for Type 2A waters (MPW-9). Depending on the contribution of the evaporitic component to reduced MNT groundwaters the redox state is variably shifted from Fe(III)/SO_4 reducing conditions (Type 1A) towards O_2-reducing conditions (Fig. 8). Type 1 waters that contain only a minor evaporitic component have a mean Eh of −100 mV, fall within the Fe(III)/SO_4 reducing field, contain median Mn and Fe concentrations that are approximately 30 and 7 times higher, respectively, than oxidised Type 2A waters. Type 2B-2 waters, which contain up to 30% evaporitic component have an intermediate Eh (median −41 mV) value reflecting a shift from Fe(III)/SO_4 reducing conditions towards Mn(IV) reducing conditions as is reflected in the lower Fe concentration of these waters (Tables 2–4). The highly oxidising nature of the evaporitic component mixing with MNT groundwaters probably reflects limitations over the electrochemical evolution of redox state within high altitude salars due to salinity effects on microbial reduction rates (Kulp et al., 2007) and perhaps a critical shortage of oxidisable organic carbon, the principal electron donor of low temperature systems.

Whereas the enrichment pattern of trace elements within the evaporitic component are a reflection of the high pH and strongly oxidising conditions within the evaporitic salar, the mass abundances and enrichment patterns of Cl, Na, SO_4, F and to a lesser degree Li, Rb, Cs and Sr are typical of conservative evaporative enrichment trajectories for evaporitic lakes (Hardie and Eugster, 1970; Eugster and Jones, 1979), and are similar to those for the highly concentrated brines reported for the region (Risacher et al., 2003).

As noted earlier, the $^{87}Sr/^{86}Sr$ value for Type 2A waters that contain the greatest evaporitic component is similar to the mean $^{87}Sr/^{86}Sr$ value for Socompa lavas and in conjunction with the enrichment in elements typical of volcanic/fumarolic sulfur mineralisation and thermal springs (Risacher et al., 2003; Banks et al., 2004) supports the origin of inflows from within the volcanic arc from one or more of the volcanoes Socompa, Salín or Pular.

Summarising, the chemical composition of the evaporitic component most evident in Type 2A groundwaters of the MNT aquifer suggest evolution within an oxidising high pH evaporitic lake receiving inflows enriched in volcanically derived species, probably from one or more of the volcanoes Socompa, Salín or Pular. Species that are unstable under these conditions are removed from solution by precipitation or co-precipitation within the shallow lake environment, whereas highly mobile oxyanions and conservative species are concentrated within the liquid phase and leak to regional groundwaters as highly oxidised evaporitic brines.

5.4. Evaporitic flow path?

Identification of the exact physical flow path for evaporitic salts mixing within the Monturaqui portion of the aquifer system is equivocal. However, on the basis of existing hydrochemical, isotopic and hydrogeological information we propose that: (i) the evaporitic component originates on the eastern side of the volcanic front within salar(s) that receive mineralised inflows from the volcanic arc (volcanoes Socompa, Salín and Pular), and; (ii) evaporitic brines from basal leakage are entrained by sub-regional groundwater flow originating within the high altiplano that subsequently flow beneath the volcanic arc, via the Salín Formation, into the Monturaqui portion of the aquifer system (Fig. 12).

Anderson et al. (2002) used a variety of techniques to estimate both recharge rate and recharge distribution to the MNT aquifer and associated the bulk of recharge with high altitude precipitation events (>4000 m) along the volcanic front and within the high altiplano with little if any effective recharge at the lower altitudes of the MNT trough. van Wyk de Vries et al. (2001) reasoned for the existence of a natural groundwater flow path originating within the high altiplano that flows beneath Volcano Socompa on the basis of topographic relief and a broad paleo-valley descending from the east. Groundwater within the Salín Formation beneath Volcano Socompa was implicated in the sagging, faulting and eventual sector collapse of the volcano (van Wyk de Vries et al., 2001). Continuous groundwater inflows along the SE margin of the Monturaqui Valley and between the low saddle separating Volcano Socompa and Volcano Pular were identified by Anderson et al. (2002). The saddle constitutes a relative broad inflow boundary ~8–10 km wide that encompasses the physical spread of the well field (Fig. 12).

Wells MPW-9–15 and 21 are directly oriented to the inferred inflow but only wells MPW-9, 14 and 15, all Type 2 waters, contain a significant evaporitic component (Fig. 10). The latter three wells all occur outside the sheltering influence of the Negrillar Volcanics. As noted in previous

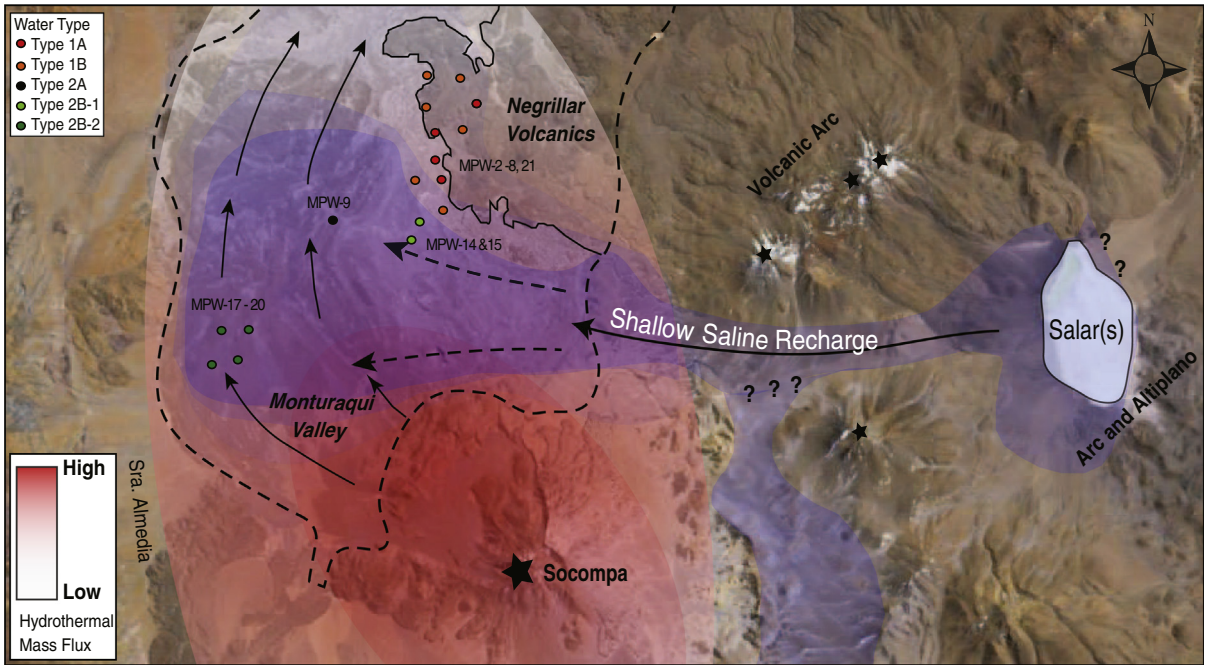

Fig. 12. Conceptual model of the origin and mixing of solute sources with the MNT aquifer system. Mass flux gradient for secondary, hydrothermal vapour phase efflux associated with Volcano Socompa is shaded in red with decreasing mass flux to the shallow meteoric aquifer with distance from the volcanic edifice. The approximate flow path of a shallow saline recharge from outside the topographic extent of the aquifer system is shaded in blue. Evaporitic salts mix with shallow meteoric groundwaters that are strongly influenced by low level vapour phase flux of hydrothermal fluids from a deep hydrothermal system associated with Volcano Socompa (Type 2 waters). The low permeability of the Negrillar Volcanics restricts mixing of liquid phase evaporitic recharge and these Type 1 waters groundwaters exhibit a dominantly peripheral bicarbonate signature. Dashed outline depicts the extent of the MNT system. (For interpretation of the references to colour in this figure legend, the reader is referred to the web version of this article.)

sections, the minor evaporitic content of groundwaters sampled from within the Negrillar Volcanics (Type 1 waters) is consistent with the presence of low permeability vents and dykes of Negrillar Volcanics acting as localised barriers to evaporitic containing inflows from the east. Southernmost production wells, MPW-17–20, that are distal from the Negrillar Volcanics also contain elevated evaporitic salt contents suggesting that the inflow(s) containing dissolved evaporitic salts are potentially laterally extensive in nature. However, well construction logs indicate that the evaporitic load of Type 2 waters is a factor of screen depth with the shallower intakes within the Salín Formation containing a greater evaporitic load. The latter suggests the restriction of the evaporitic component to specific horizon permeable layers within the upper layers of the Salín Formation with the exception of the Negrillar Volcanics where the intrusion of volcanic dykes and vents partially or wholly block the ingress of evaporitic solutes.

The absence of current evaporitic salars within the topographic bounds of the MNT aquifer system exerts a fundamental constraint over the origin of the evaporitic component mixing within the MNT aquifer system. Furthermore, the persistence of buried evaporites along aquifer flow paths as the source of evaporitic salts to the MNT aquifer was thought unlikely given the age of the aquifer system (Miocene–Pleistocene) and current high aquifer throughput (higher during pluvial periods) with both factors suggesting any buried brines would have been exhausted long before sampling. Where the water table lies, ca. 100 m b.g.l., the units of the Salín Formation aquifer pre-date sector collapse of Volcano Socompa and probably the volcano itself meaning more than sufficient time and fresh throughput to have occurred for the exhaustion of any buried brines. A similar argument for rapid exhaustion of buried evaporitic brines was proposed by Risacher et al. (2003) who calculated between 100 years to 1.7 million years for the saline brines of a buried salar to be exhausted by fresh inflows for small (10 km^2) and large (150 km^2) salars of the region, respectively. Rapid depletion of buried evaporitic brines along aquifer flow paths is not surprising given both the high solubility of these salts and high aquifer throughput.

In summary, hydrogeological, chemical and isotopic data support the existence of a broad inflow of shallow groundwater originating from the east. A portion of this inflow originates from beyond the topographic boundary of the MNT aquifer and carries with it a significant evaporitic load that mixes with dilute meteoric groundwaters influenced by localised hydrothermal activity associated with Volcano Socompa.

6. Conclusions

Based on our work and the hydrogeological setting of the MNT aquifer system we propose a conceptual model for the solute sources and hydrochemical evolution of MNT groundwaters (Fig. 12). Specifically, local and regional scale evidence supports our hypothesis of mixing between: (i) meteoric groundwaters influenced by relatively low level diffuse degassing of vapour phase constituents associated with an underlying volcanic-hydrothermal system (Volcano Socompa), and: (ii) an alkaline, oxidising, evaporitic brine probably originating within the volcanic arc/high altiplano.

If the contribution from saline evaporitic inflows are excluded, the composition of MNT groundwaters are typical of what would be expected at the extreme distal margins of a convecting hydrothermal system where the transition between secondary hydrothermal and meteoric alteration is driven by steep gradients in heat and mass flow (Giggenbach, 1981, 1984, 1988). The existence of a heat source driving a convecting hydrothermal system beneath Volcano Socompa is consistent with the relatively recent formation of dome complexes within the collapse scar, at ~5250 yr B.P., and the available information on thermal gradients and fluxes around magmatic intrusions that suggest cooling times on the order of 10^6 years (Ingebritsen et al., 2001; Deckart et al., 2005). Within this setting, the dominant Na–HCO_3 hydrochemical facies of MNT groundwaters are designated as dilute peripheral bicarbonate waters which reflect the separation of a CO_2 rich vapour phase boiled off an underlying hydrothermal reservoir and its absorption in the shallow meteoric groundwaters of the MNT aquifer system (Giggenbach,

1981, 1988). The absence of oxygen within these waters limits the oxidation of H_2S with the bulk of acidity due to dissociation of H_2CO_3.

Adsorption of CO_2 generates an environment of minor acid alteration and furnishes MNT groundwaters with cations derived from local host rocks, producing low Cl waters relatively high in bicarbonate and low in SO_4 as is exemplified by Type 1A waters (MPW-5). With distance from Socompa, hydrothermal mass and heat flux wane along with the signature of secondary hydrothermal alteration with meteoric interaction becoming proportionately more important within Type 1A groundwaters occurring within the sheltered Negrillar Volcanics.

Solutes derived from localised secondary gas–water–rock interaction then mix with increasing proportions of oxidising evaporitic solutes rich in SO_4 with the relative contribution of evaporitic solutes increasing along the continuum of groundwater types: 1B ≫ 2B-1 > 2B-2 ≫ 2A (Fig. 10). The introduction of evaporitic SO_4 and Cl shifts the hydrochemical facies of MNT groundwaters towards the dilute SO_4–Cl end member as well as producing a proportionate shift in redox potential towards more oxidising conditions (Fig. 8).

Hydrogeological and chemical data indicate the existence of an extra-basinal flow path containing elevated concentrations of evaporitic salts originating within the high altiplano (Fig. 12). Spatially, the inflows containing the evaporitic component appear to be laterally diffuse but vertically restricted to horizon permeable layers within the upper layers of the Salín Formation. The low permeability vents and dykes of the Negrillar Volcanics form a localised barrier to evaporite-enriched groundwaters originating from the east and host relatively dilute groundwaters (Type 1) consistent with low grade hydrogen metasomatism of volcanic rock. Ultimately, solutes derived from meteoric, hydrothermal and evaporitic sources mix within the MNT aquifer system and discharge to the Salar de Atacama.

Acknowledgements

We thank BHP-Billiton for permission to sample from their well field in the MNT, for logistical support, and for funding the fieldwork and geochemical analyses. Tim Denison is thanked for assistance with the Sr isotope analyses, and Dan Layton-Matthews for discussions and assistance with the ICP-MS analyses. We thank journal editor Michael E. Böttcher and two anonymous reviewers for constructive comments that greatly improved the paper.

References

Alpers, C.N., Brimhall, G.H., 1988. Middle Miocene climatic change in the Atacama Desert, northern Chile: evidence from supergene mineralization at La Escondida. Geol. Soc. Am. Bull. 100, 1640–1656.

Alpers, C.N., Whittemore, D.O., 1990. Hydrochemistry and stable isotopes of ground and surface waters from two adjacent closed basins, Atacama Desert, northern Chile. Appl. Geochem. 5, 719–734.

Anderson, M., Low, R., Foot, S., 2002. Sustainable groundwater development in arid, high Andean basins. In: Hiscock, K.M., Rivett, M.O., Davidson, R.M. (Eds.), Sustainable Groundwater Development. Geological Society of London Special Publication, pp. 133–144.

Arancibia, G., Matthews, S.J., De Arce, C.P., 2006. K–Ar and $^{40}Ar/^{39}Ar$ geochronology of supergene processes in the Atacama Desert, Northern Chile: tectonic and climatic relations. J. Geol. Soc. 163, 107–118.

Aravena, R., Suzuki, O., 1990. Isotopic evolution of river water in the northern Chile region. Water Resour. Res. 26, 2887–2895.

Aravena, R., Suzuki, O., Pena, H., Pollastri, A., Fuenzalida, H., Grilli, A., 1999. Isotopic composition and origin of the precipitation in northern Chile. Appl. Geochem. 14, 411–422.

Banks, D., Parnachev, V.P., Frengstad, B., Holden, W., Karnachuk, O.V., Vedernikov, A.A., 2004. The evolution of alkaline, saline ground- and surface waters in the southern Siberian steppes. Appl. Geochem. 19, 1905–1926.

Bethke, C.M., 2008. The Geochemist's Workbench. University of Illinois.

Bock, B., Bahlburg, H., Worner, G., Zimmermann, U., 2000. Tracing crustal evolution in the southern central Andes from Late Precambrian to Permian with geochemical and Nd and Pb isotope data. J. Geol. 108 (5), 515–535.

Boschetti, T., Cortecci, G., Barbieri, M., Mussi, M., 2007. New and past geochemical data on fresh to brine waters of the Salar de Atacama and Andean Altiplano, northern Chile. Geofluids 7 (1), 33–50.

Burke, W.H., Hetherington, E.A., 1984. Normalized $^{87}Sr/^{86}Sr$ by multiple collection and comparison to a standard. Chem. Geol. 46, 265–268.

Cameron, E.M., Leybourne, M.I., 2005. Relationship between groundwater chemistry and soil geochemical anomalies at the Spence copper porphyry deposit, Chile. Geochem. Explor. Environ. Anal. 5, 135–145.

Capaccioni, B., Aguilera, F., Tassi, F., Darrah, T., Poreda, R.J., Vaselli, O., 2011. Geochemical and isotopic evidences of magmatic inputs in the hydrothermal reservoir feeding the fumarolic discharges of Tacora volcano (northern Chile). J. Volcanol. Geotherm. Res. 208 (3–4), 77–85.

Cheatham, M.M., Sangrey, W.F., White, W.M., 1993. Sources of error in internal calibration ICP-MS analysis of geological samples and an improved non-linear drift correction procedure. Spectrochimica Acta 48B, E487–E506.

Clark, I.D., Fritz, P., 1997. Environmental Isotopes in Hydrogeology. Lewis Publishers, Boca Raton, New York (328 pp.).

Clarke, J.D.A., 2006. Antiquity of aridity in the Chilean Atacama Desert. Geomorphology 73 (1–2), 101–114.

Cortecci, G., Boschetti, T., Mussi, M., Lameli, C.H., Mucchino, C., Barbieri, M., 2005. New chemical and original isotopic data on waters from El Tatio geothermal field, northern Chile. Geochem. J. 39 (6), 547–571.

Costello, E.K., Halloy, S.R.P., Reed, S.C., Sowell, P., Schmidt, S.K., 2009. Fumarole-supported islands of biodiversity within a hyperarid, high-elevation landscape on Socompa Volcano, Puna de Atacama, Andes. Appl. Environ. Microbiol. 75 (3), 735–747.

Craig, H., 1961. Isotopic variations in meteoric waters. Science 133, 1702–1703.

Daughney, C.J., Raiber, M., Moreau-Fournier, M., Morgenstern, U., van der Raaij, R., 2012. Use of hierarchical cluster analysis to assess the representativeness of a baseline groundwater quality monitoring network: Comparison of New Zealand's national and regional groundwater monitoring programs. Hydrogeology Journal 20 (1), 185–200.

de Silva, S.L., Francis, P.W., 1991. Volcanoes of the Central Andes. Springer-Verlag, New York.

Deckart, K., Clark, A.H., Aguilar, A.C., Vargas, R.R., Bertens, A.N., Mortensen, J.K., Fanning, M., 2005. Magmatic and hydrothermal chronology of the Giant Río Blanco porphyry copper deposit, central Chile: implications of an integrated U–Pb and $^{40}Ar/^{39}Ar$ database. Econ. Geol. 100 (5), 905–934.

Delany, J.M., Lundeen, S.R., 1989. The LLNL thermodynamic database Lawrence Livermore National Laboratory Report UCRL-21658 (1989).

DeMaster, D.J., 2004. The diagenesis of biogenic silica: chemical transformations occurring in the water column, seabed, and crust. In: Mackenzie, F.T. (Ed.), Treatise of Geochemistry, pp. 87–98.

Deocampo, D.M., 2005. Evaporative evolution of surface waters and the role of aqueous CO_2 in magnesium silicate precipitation: Lake Eyasi and Ngorongoro crater, northern Tanzania. S. Afr. J. Geol. 108 (4), 493–504.

Déruelle, B., 1978a. The Negros de Aras nuee ardente deposits; a cataclysmic eruption of Socompa Volcano (Andes of Atacama, Chile). Bull. Volcanol. 41 (3), 175–186.

Déruelle, B., 1978b. Calc-alkaline and shoshonitic lavas from five Andean volcanoes (between latitudes 21°45′ and 24°30′S) and the distribution of the Plio-Quaternary volcanism of the south-central and southern Andes. J. Volcanol. Geotherm. Res. 3 (3–4), 281–298.

Déruelle, B., Moorbath, S., 1993. A similar magma source for ignimbrites and non-ignimbritic lavas from South-Central Andes, Andean Geodynamics. Proceedings of the ORSTOM/Oxford University International Symposium (Oxford), pp. 351–354.

Déruelle, B., Figueroa, A.O., Medina, T.E., Viramonte, G.J., Maragaño, C.M., 1996. Petrology of pumices of April 1993 eruption of Lascar (Atacama, Chile). Terra Nova 8 (2), 191–199.

Drees, K.P., Neilson, J.W., Betancourt, J.L., Quade, J., Henderson, D.A., Pryor, B.M., Maier, R.M., 2006. Bacterial community structure in the hyperarid core of the Atacama Desert, Chile. Appl. Environ. Microbiol. 72 (12), 7902–7908.

Drever, J.I., 1997. The Geochemistry of Natural Waters. Prentice-Hall, Englewood Cliffs, NJ, United States (436 pp.).

Dunai, T.J., Lopez, G.A.G., Juez-Larre, J., 2005. Oligocene–Miocene age of aridity in the Atacama Desert revealed by exposure dating of erosion-sensitive landforms. Geology 33 (4), 321–324.

Eugster, H.P., Jones, B.F., 1979. Behavior of major solutes during closed basin — lakes brine evolution. Am. J. Sci. 279 (6), 609–631.

Farias, M.E., Revale, S., Mancini, E., Ordoñez, O., Turjanski, A., Cortez, N., Vazquez, M.P., 2011. Genome sequence of *Sphingomonas* sp. S17, isolated from an Alkaline, hyperarsenic, and hypersaline volcano-associated lake at high altitude in the Argentinean Puna. J. Bacteriol. 193 (14), 3686–3687.

Faure, G., 1986. Principles of Isotope Geology. Wiley and Sons, New York 589 pp.

Federico, C., Aiuppa, A., Allard, P., Bellomo, S., Jean-Baptiste, P., Parello, F., Valenza, M., 2002. Magma-derived gas influx and water–rock interactiosn in the volcanic aquifer of Mt. Vesuvius, Italy. Geochim. Cosmochim. Acta 66, 963–981.

Fetter, C.W., 1994. Applied Hydrogeology. Macmillan, New York (691 pp.).

Fischer, T.P., Giggenbach, W.F., Sano, Y., Williams, S.N., 1998. Fluxes and sources of volatiles discharged from Kudryavy, a subduction zone volcano, Kurile Islands. Earth Planet. Sci. Lett. 160, 81–96.

Francis, P.W., Gardeweg, M., Ramirez, C.F., Rothery, D.A., 1985. Catastrophic debris avalanche deposit of Socompa volcano, northern Chile. Geology 13 (9), 600–603.

Fritz, P., Suzuki, O., Silva, C., Salati, E., 1981. Isotope hydrology of groundwaters in the Pampa Del Tamarugal, Chile. J. Hydrol. 53, 161–184.

Garrels, R.M., Christ, C.L., 1965. Solutions, Minerals, and Equilibria. Freeman, Cooper & Co., San Francisco (450 pp.).

Giggenbach, W.F., 1981. Gothermal mineral equilibra. Geochim. Cosmochim. Acta 45, 393–410.

Giggenbach, W.F., 1984. Mass-transfer in hydrothermal alteration systems. Geochim. Cosmochim. Acta 48, 2693–2713.

Giggenbach, W.F., 1988. Geothermal solute equilibria. Derivation of Na–K–Mg–Ca geoindicators. Geochim. Cosmochim. Acta 52, 2749–2765.
Ginot, P., Kull, C., Schotterer, U., Schwikowski, M., Gäggeler, H.W., 2006. Glacier mass balance reconstruction by sublimation induced enrichment of chemical species on Cerro Tapado (Chilean Andes). Clim. Past 2 (1), 21–30.
Güler, C., Thyne, G.D., McCray, J.E., Turner, A.K., 2002. Evaluation of graphical and multivariate statistical methods for classification of water chemistry data. Hydrogeology Journal 10 (4), 455–474.
Hamamura, N., Liy, Y., Inskeep, W.P., 2012. Identification of bacterial community and arsenate-reducing bacteria associated with a soda lake in Khovsgol, Mongolia. In: Kawaguchi, M., et al. (Eds.), Interdisciplinary Studies on Environmental Chemistry—Environmental Pollution and Ecotoxicology. Terrapub, pp. 99–107.
Hardie, L.A., Eugster, H.P., 1970. The evolution of closed-basin brines. Miner. Soc. Am. Spec. Pap. 3, 273–290.
Hards, V., 2005. Volcanic contributions to the global carbon cycle. Brit. Geol. Surv. 20.
Hartley, A.J., Chong, G., 2002. Late Pliocene age for the Atacama Desert: implications for the desertification of western South America. Geology 30 (1), 43–46.
Hartley, A.J., Rice, C.M., 2005. Controls on supergene enrichment of porphyry copper deposits in the central Andes: a review and discussion. Mineral. Deposita 40, 515–525.
Hem, J.D., 1985. Study and interpretation of the chemical characteristics of natural water. US Geological Survey Water-Supply Paper 2254.
Herrera, V., De Gregori, I., Pinochet, H., 2009. Assesment of trace elements and mobility of arsenic and manganese in Lagoon sediments of the Huasco and Coposa salt flats, Chilean altiplano. J. Chil. Chem. Soc. 54 (4), 454–459.
Ingebritsen, S.E., Galloway, D.L., Colvard, E.M., Sorey, M.L., Mariner, R.H., 2001. Time-variation of hydrothermal discharge at selected sites in the Western United States: implications for monitoring. J. Volcanol. Geotherm. Res. 111 (1–4), 1–23.
Karim, M.R.A., 1998. Pumping test re-analysis. The University of Birmingham, School of Engineering Report, Monturaqui Basine, Chile, 16 p.
Katz, B.G., Catches, J.S., Bullen, T.D., Michel, R.L., 1998. Changes in the isotopic and chemical composition of ground water resulting from a recharge pulse from a sinking stream. Journal of Hydrology 211 (1–4), 178–207.
Kesler, S.E., Gruber, P.W., Medina, P.A., Keoleian, G.A., Everson, M.P., Wallington, T.J., 2012. Global lithium resources: relative importance of pegmatite, brine and other deposits. Ore Geol. Rev. 48, 55–69.
Kiyosu, Y., Kurahashi, M., 1983. Origin of sulfur species in acid sulfate–chloride thermal waters, northeastern Japan. Geochim. Cosmochim. Acta 47 (7), 1237–1245.
Kraemer, B., Wittenbrink, R., Hahne, K., Gertsenberger, H., 1996. Geochemical constraints on crustal structure from Neogene volcanic rocks of the Salar de Antofalla volcanic field and adjacent Andean Cordillera (24°–26°S, 67°–69°W). Third International Symposium on Andean Geodynamics, St. Malo, France, pp. 589–592.
Krouse, H.R., 1974. Sulphur isotope variations in thermal and mineral waters. In: Cadek, J., Paces, T. (Eds.), International Symposium on Water–Rock Interaction. The Geological Survey, Prague, Former Republich of Czechoslovakia.
Krouse, H.R., 1976. Sulphur isotope variations in thermal and mineral waters. In: Cadek, J., Paces, T. (Eds.), Proceedings: International Symposium on Water–Rock Interaction. Geological Survey, Prague, pp. 340–347.
Kulp, T.R., Han, S., Saltikov, C.W., Lanoil, B.D., Zargar, K., Oremland, R.S., 2007. Effects of imposed salinity gradients on dissimilatory arsenate reduction, sulfate reduction, and other microbial processes in sediments from two California soda lakes. Appl. Environ. Microbiol. 73 (16), 5130–5137.
Kusakabe, M., Komoda, Y., Takano, B., Abiko, T., 2000. Sulfur isotopic effects in the disproportionation reaction of sulfur dioxide in hydrothermal fluids: implications for the $\delta^{34}S$ variations of dissolved bisulfate and elemental sulfur from active crater lakes. J. Volcanol. Geotherm. Res. 97 (1–4), 287–307.
Lewicki, J.L., Fischer, T., Williams, S.N., 2000. Chemical and isotopic compositions of fluids at Cumbal Volcano, Columbia: evidence for magmatic contribution. Bull. Volcanol. 62, 347–361.
Leybourne, M.I., Cameron, E.M., 2006. Composition of groundwaters associated with porphyry-Cu deposits, Atacama Desert, Chile: elemental and isotopic constraints on water sources and water–rock reactions. Geochim. Cosmochim. Acta 70, 1616–1635.
Leybourne, M.I., Cameron, E.M., 2008. Source, transport, and fate of rhenium, selenium, molybdenum, arsenic, and copper in groundwater associated with porphyry-Cu deposits, Atacama Desert, Chile. Chem. Geol. 247, 208–228.
Leybourne, M.I., Cameron, E.M., Reich, M., Palacios, C., Faure, K., Johannesson, K.H., 2013. Stable isotopic composition of soil calcite (O, C) and gypsum (S) overlying Cu deposits in the Atacama Desert, Chile: implications for mineral exploration, salt sources, and paleoenvironmental reconstruction. Appl. Geochem. 29, 55–72.
Macpherson, G.L., 2009. CO2 distribution in groundwater and the impact of groundwater extraction on the global C cycle. Chemical Geology 264 (1–4), 328–336.
Magaritz, M., Aravena, R., Peña, H., Suzuki, O., Grilli, A., 1989. Water chemistry and isotopic study of streams and springs in northern Chile. J. Hydrol. 108, 323–341.
Magaritz, M., Aravena, R., Peña, H., Suzuki, O., Grilli, A., 1990. Source of ground water in the deserts of northern Chile: evidence of deep circulation of ground water from the Andes. Ground Water 28, 513–517.
Mamani, M., Tassara, A., Wörner, G., 2008. Composition and structural control of crustal domains in the central Andes. Geochem. Geophys. Geosyst. 9 (3).
Marini, L., Gambardella, B., 2005. Geochemical modeling of magmatic gas scrubbing. Ann. Geophys. 48 (4–5), 739–753.
Marini, L., Ottonello, G., Canepa, M., Cipolli, F., 2000. Water–rock interaction in the Bisagno valley (Genoa, Italy): application of an inverse approach to model spring water chemistry. Geochim. Cosmochim. Acta 64 (15), 2617–2635.
Masscheleyn, P.H., Delaune, R.D., Patrick Jr., W.H., 1991. Effect of redox potential and pH on arsenic speciation and solubility in a contaminated soil. Environ. Sci. Technol. 25 (8), 1414–1419.
McArthur, J.M., Howarth, R.J., 2004. Strontium isotope stratigraphy. In: F.M., G., Ogg, J.G., Smith, A.G. (Eds.), A Geologic Timescale 2004. Cambridge University Press, pp. 96–105.
Miller, A., 1976. The climate of Chile. In: Schwerdtfeger, W. (Ed.), Climates of Central and South America.
Morford, J.L., Emerson, S.R., Breckel, E.J., Kim, S.H., 2005. Diagenesis of oxyanions (V, U, Re, and Mo) in pore waters and sediments from a continental margin. Geochim. Cosmochim. Acta 69 (21), 5021–5032.
Oremland, R.S., Stolz, J.F., Hollibaugh, J.T., 2004. The microbial arsenic cycle in Mono Lake, California. FEMS Microbiol. Ecol. 48 (1), 15–27.
Peña, H., Grilli, A., Salazar, C., Orphanopoulos, D., Suzuki, O., Aravena, R., Rauert, W., 1989. Estudio de Hidrologia isotopica en al area del Salar de Llamara, Desierto de Atacama, Chile. Proc. Symp. Isotope Hydrology Investigations in Latin America, IAEA-TECDOC. 502, pp. 113–127.
Pueyo, J.J., Chong, G., Jensen, A., 2001. Neogene evaporites in desert volcanic environments: Atacama Desert, northern Chile. Sedimentology 48, 1411–1431.
Quade, J., Rech, J.A., Latorre, C., Betancourt, J.L., Gleeson, E., Kalin, M.T.K., 2007. Soils at the hyperarid margin: the isotopic composition of soil carbonate from the Atacama Desert, Northern Chile. Geochim. Cosmochim. Acta 71 (15), 3772–3795.
Rech, J.A., Quade, J., Betancourt, J.L., 2003. Controls on the isotopic composition of soil carbonate in a hyperarid environment; a case study from the Atacama Desert, Chile. Geological Society of America, 2003 Annual Meeting, Geological Society of America, 2003 Annual Meeting, Seattle, WA, United States, Nov. 2–5, 2003, p. 408.
Rech, J.A., Currie, B.S., Michalski, G., Cowan, A.M., 2006. Neogene climate change and uplift in the Atacama Desert, Chile. Geology 34 (9), 761–764.
Reich, M., Palacios, C., Vargas, G., Luo, S., Cameron, E.M., Leybourne, M.I., Parada, M.A., Zuniga, A., You, C.F., 2009. Supergene enrichment of copper deposits since the onset of modern hyperaridity in the Atacama Desert, Chile. Mineral. Deposita 44 (5), 497–504.
Risacher, F., Alonso, H., 2001. Geochemistry of ash leachates from the 1993 Lascar eruption, northern Chile. Implication for recycling of ancient evaporites. J. Volcanol. Geotherm. Res. 109 (4), 319–337.
Risacher, F., Fritz, B., 1991. Geochemistry of Bolivian salars, Lipez, southern Altiplano: origin of solutes and brine evolution. Geochim. Cosmochim. Acta 55, 687–705.
Risacher, F., Fritz, B., 2008. Origin of salts and brine evolution of Bolivian and Chilean salars. Aquat. Geochem. 15, 123–157.
Risacher, F., Alonso, H., Salazar, C., 2003. The origins of brines and salts in Chilean salars: a hydrochemical review. Earth Sci. Rev. 63, 249–293.
Risacher, F., Fritz, B., Hauser, A., 2011. Origin of components in Chilean thermal waters. J. S. Am. Earth Sci. 31 (1), 153–170.
Rissmann, C., Christenson, B., Werner, C., Leybourne, M., Cole, J., Gravley, D., 2012. Surface heat flow and CO_2 emissions within the Ohaaki hydrothermal field, Taupo Volcanic Zone, New Zealand. Appl. Geochem. 27 (1), 223–239.
Schoen, R., Rye, R.O., 1970. Sulfur isotope distribution in solfataras, yellowstone national park. Science 170 (3962), 1082–1084.
Siebert, L., Simkin, T., 2002. Volcanoes of the world: an illustrated catalog of Holocene volcanoes and their eruptions. Smithsonian Institution, Global Volcanism Program Digital Information Series, GVP-3 (http://www.volcano.si.edu/world/).
Spiro, B., Chong, G., 1996. Origin of sulfate in the Salar de Atacama and the Cordillera de la Sal: initial results of an isotopic study. Third International Symposium on Andean Geodynamics, ORSTOM, St. Malo, France, pp. 703–706.
Spiro, B., Hoke, L., Chenery, C., 1997. Carbon-isotope characteristics of CO_2 and CH_4 in geothermal springs from the Central Andes. Int. Geol. Rev. 39 (10), 938–947.
Stichler, W., Schotterer, U., Fröhlich, K., Ginot, P., Kull, C., Gäggeler, H., Pouyaud, B., 2001. Influence of sublimation on stable isotope records recovered from high-altitude glaciers in the tropical Andes. J. Geophys. Res. D Atmos. 106 (D19), 22613–22620.
Tassi, F., Aguilera, F., Darrah, T., Vaselli, O., Capaccioni, B., Poreda, R.J., Delgado Huertas, A., 2010. Fluid geochemistry of hydrothermal systems in the Arica–Parinacota, Tarapacá and Antofagasta regions (northern Chile). J. Volcanol. Geotherm. Res. 192 (1–2), 1–15.
van Wyk de Vries, B., Self, S., Francis, P.W., Keszthelyi, L., 2001. A gravitational spreading origin for the Socompa debris avalanche. J. Volcanol. Geotherm. Res. 105 (3), 225–247.
Wadge, G., Francis, P.W., Ramirez, C.F., 1995. The Socompa collapse and avalanche event. J. Volcanol. Geotherm. Res. 66 (1–4), 309–336.
Youngman, K.J., 1984. Hydrothermal Alteration and Fluid–Rock Interaction in the El Tatio Geothermal Field, Antofagasta Province, Chile, University of Auckland (123 pp.).
Zhang, J., Quay, P.D., Wilbur, D.O., 1995. Carbon-isotope fractionation during gas–water exchange and dissolution of CO_2. Geochim. Cosmochim. Acta 59 (1), 107–114.